



# CHALMERS

---

## Simulation of Heat Integration in Exhaust After Treatment for Dual-Fuel Vehicles

*Master's Thesis in the Master programs Innovative and Sustainable Chemical Engineering and  
Engineering Mathematics*

JOHANNES BRANDT  
HENRIK DROTTZ

Department of Chemical and Biological Engineering  
CHALMERS UNIVERSITY OF TECHNOLOGY  
Gothenburg, Sweden 2014  
Master's Thesis 2014:06



MASTER'S THESIS IN CHEMICAL ENGINEERING

# Simulation of Heat Integration in Exhaust After Treatment for Dual-Fuel Vehicles

JOHANNES BRANDT & HENRIK DROTTZ

Department of Chemical and Biological Engineering  
*Division of Chemical Engineering*

CHALMERS UNIVERSITY OF TECHNOLOGY  
Gothenburg, Sweden 2014



Simulation of Heat Integration in Exhaust After Treatment for Dual-Fuel Vehicles  
JOHANNES BRANDT & HENRIK DROTTZ

©JOHANNES BRANDT & HENRIK DROTTZ, 2014

Master's Thesis 2014:06  
Department of Chemical Engineering  
Chalmers University of Technology  
SE-412 96 Gothenburg  
Sweden  
Telephone: +46 (0)31-772 1000

Chalmers Reproservice/Department of Chemical Engineering  
Gothenburg, Sweden 2014



## Abstract

The main objective of this thesis is to analyze exhaust after treatment systems that can reduce methane emissions from a dual fuel (gas/diesel) engine by the use of heat integration. Numerical simulations of an exhaust after treatment system over a truck have been conducted by using different simulation methods. CFD simulations over different geometrical setups of plate heat exchangers have been performed using ANSYS 15.0.0 and heat integration analyses over a heat exchanger-catalyst system has been conducted with the use of Matlab. The CFD simulations showed that even small distances between the plates of the heat exchanger affects the convective heat transfer coefficient of the system, compared to when the plates are in contact. CFD simulations were conducted over different widths of the heat exchanger from which it could be concluded that the Reynolds number as well as geometrical properties such as the Chevron angle of the heat exchanger played a vital part when deciding a proper width of the simulated segment. By performing transient simulations of typical driving conditions for a truck, it was concluded that the concept of a sequential heat exchanger-catalyst system showed potential in preserving the temperature within the catalyst, sufficiently high for the methane to be converted. However additional heating would be needed during the cold start period.

Keywords: *exhaust after treatment, dual fuel, plate heat exchanger, heat integration, CFD*



## **Preface**

This Master of Science thesis has been performed by Johannes Brandt and Henrik Drottz, students at the Master's program Engineering Mathematics and Innovative and Sustainable Chemical Engineering at Chalmers University of Technology, Gothenburg, Sweden. The thesis has been performed within the MEGAS project, which is founded the Swedish Energy Agency, and it has been in collaboration with Volvo Group Trucks Technology and the department of Chemical Engineering at Chalmers University of Technology. It was supervised by Dr. Martin Lundén and Dr. Anna Lindholm at Volvo. The examiner and supervisor at Chalmers University of Technology was assistant professor Ronnie Andersson.

## **Acknowledgements**

We would like to thank our supervisor assistant professor Ronnie Andersson for helping us with the technical problems encountered during the thesis. We want to thank Dr. Martin Lundén for all his meetings with us, where we got many ideas on how to proceed with our work, as well as Dr. Anna Lindholm for her ideas to the thesis. Finally, we would like to thank Volvo Group Trucks Technology for giving us the opportunity for working together with them and for the Swedish Energy Agency for providing funding for the MEGAS project, thereby enabling this thesis work.

Johannes Brandt & Henrik Drottz, Gothenburg 2014-06

# Contents

<b>1</b>	<b>Introduction</b>	<b>1</b>
<b>2</b>	<b>Heat Integration</b>	<b>1</b>
2.1	Coated Heat Exchanger . . . . .	2
2.2	Integrated and Sequential Heat Exchangers . . . . .	3
<b>3</b>	<b>Theory and Simulation Methods</b>	<b>7</b>
3.1	Heat Exchangers . . . . .	8
3.1.1	Plate Heat Exchanger Corrugations . . . . .	8
3.1.2	Chevron Angles . . . . .	9
3.1.3	Flow Properties . . . . .	11
3.1.4	Correlations . . . . .	11
3.1.5	Steady State Model . . . . .	12
3.2	Transient Response of a heat exchanger . . . . .	13
3.2.1	Boundary Conditions . . . . .	15
3.2.2	Solution Procedure . . . . .	16
3.2.3	Modeling the Catalyst . . . . .	18
3.2.4	Solving for Both the Heat Exchanger and the Catalyst . . . . .	19
3.2.5	Response in Time Domain . . . . .	20
3.2.6	Implementation . . . . .	21
3.2.7	Error Analysis . . . . .	21
3.3	CFD Simulation of a Heat Exchanger . . . . .	21
3.3.1	Governing Equations . . . . .	22
3.3.2	Turbulence Modeling . . . . .	22
3.3.3	The k- $\omega$ SST model . . . . .	23
3.3.4	Simulations Methodology . . . . .	24
3.3.5	Boundary Conditions for the Simulations . . . . .	25
3.3.6	Simulated Geometries . . . . .	26
<b>4</b>	<b>Results</b>	<b>29</b>
4.1	System Simulations-Steady State Condition . . . . .	29
4.2	System Simulations - Transient Analysis . . . . .	31
4.2.1	Evaluation of the Accuracy and parameter Sensitivity of the Transient Model . . . . .	35
4.2.2	Calculation time . . . . .	37
4.3	CFD Simulations . . . . .	38
<b>5</b>	<b>Discussion</b>	<b>42</b>
5.1	Transient Simulations . . . . .	42
5.2	CFD . . . . .	43
<b>6</b>	<b>Conclusions</b>	<b>44</b>
<b>7</b>	<b>Future Work</b>	<b>45</b>

Symbol	Units	Description
$a$	–	Constant in the Laplace inversion formula
$A$	$m^2$	Projected heat transfer area per plate
$\bar{A}$	–	Coefficient matrix for system of differential equations
$A_c$	$m^2$	Free flow area in a channel
$B$	$m$	Width
$C$	$J/K$	Heat Capacity of resident fluid
$c_m$	$mol/m^3$	Concentration methane
$c_p$	$J/(kg \cdot K)$	Heat Capacity
$d_j$	–	Constants to be determined by boundary conditions
$D$	$m^2/s$	Diffusivity
$G$	–	$a/2t$
$h$	$W/(m^2 \cdot K)$	Convective heat transfer coefficient
$k$	$W/(m \cdot K)$	Thermal conductivity
$k_m$	$m/s$	Mass transport coefficient
$L$	$m$	Length
$\dot{m}$	$kg/s$	Mass flow rate
$R_c$	–	Wall heat capacity ratio, $C_w/C$
$s$	–	Transformed variable in Laplace domain
$t$	–	Dimensionless time
$T$	–	Dimensionless temperature
$\hat{T}$	–	Laplace transform of temperature term
$u_j$	–	eigenvectors of matrix $\bar{A}$
$U$	$W/(m^2 \cdot K)$	Overall heat transfer coefficient
$U_i$	–	Number of transfer units, $h_i A / \dot{m} c_p$
$v$	$m/s$	Velocity
$X$	–	Dimensionless length
$y$	–	mass ppm methane

Greek Symbols	Units	Description
$\beta_j$	–	$j$ th eigenvalue of matrix $\bar{A}$
$\Delta H$	$J/(mol)$	Reaction enthalpy
$\Delta H_r$	$J/(kg)$	Reaction enthalpy
$\theta$	$K$	Temperature
$\mu$	$Pa \cdot s$	Viscosity
$\rho$	$kg/m^3$	Density
$\tau$	$s$	Time
$\phi$	–	Real area divided by projected area

Subscript	Description
cat	Catalyst
i	$i$ th channel
p	Plate
w	Wall

# 1 Introduction

The vehicle emission have during the years been regulated with improved and tougher emission standards, which forces the vehicle manufactures to seek ways to lower their emissions [1]. One possible way of doing this is by changing or combining different fuel inputs to the engine. There are currently dual-fuel engines which uses a diesel and bio/natural gas combination as fuel. A benefit of using methane gas is that there is a possibility to reduce the carbon dioxide emissions [2]. In addition, natural gas is also an easy accessible fuel source compared to diesel. A drawback is however that some of the methane gas does not get combusted in the engine and therefore needs to be treated in the after treatment system of the vehicle. This is of great importance since methane is 20 times as potent as carbon dioxide regarding the green house effects [3]. However methane is difficult to convert in a catalytic reactor since it requires very high temperatures for the methane to be converted. A possible solution to the problem might be with the use of heat integration.

Since methane reacts exothermically in the catalytic reactor, the idea is to use a heat exchanger to transfer the heat from the warmer outgoing stream of the catalyst to the colder incoming stream. The exhaust gas is hence first preheated, giving a higher inlet temperature to the catalyst and thus increasing the conversion of methane. In order to achieve good conversion in the catalyst, temperatures above  $400^{\circ}C$  are needed. The exhaust gas from the engine is however expected under normal driving cycles to give temperatures significantly below the light off for methane. This indicates that a large heat transfer area will be required for the heat exchanger. In the vehicle industry, this presents a problem since compact constructions are highly preferable. The heat exchanger type which is best fitted for the task is therefore the plate heat exchanger [4].

The aim of this thesis is hence to investigate if it is possible to design a plate heat exchanger so that the temperatures can be kept above  $400^{\circ}C$  in the catalyst, with the size and the pressure drop being two limiting constraints. In order to investigate the design of the plate heat exchanger a literature study is done, resulting in experimental correlations that can be used to predict the performance of the heat exchanger. To be able to easily choose any design with any flow conditions it is evaluated if it is possible to use CFD as a design tool, where various designs are compared to the experimental correlations.

A major problem when it comes to designing the heat exchanger and catalyst is that the in-data to the system, temperature, methane, and mass flow, has a very rapid changes in time. Hence to be able to predict the temperature into the catalyst a model that can handle the transient data is needed. This will be achieved by setting up balances for the heat exchanger and the catalyst, giving a system of coupled differential equations. To solve the equations a method using Laplace transform and a numeric inversion of the transform is used. The model is also used to make predictions regarding the question if additional heating will be needed during cold start.

## 2 Heat Integration

The concept of using a heat integration in order to reach higher temperatures, and hence higher methane conversion, has been studied before. Thus the aim of this section is to give a brief summary of previous ideas, and hence also give a good platform for introducing new ideas.

## 2.1 Coated Heat Exchanger

Heed and Wingård introduced the concept of a heat exchanger with integrated catalyst [5]. The heat exchanger is made of stainless steel which is folded in a zig-zag way, and impregnated with catalytic active material. Hence heat exchange and reaction take place simultaneously in the same unit. During cold start there will be no conversion of methane, but there are however other, more easily combusted, components that will heat the converter. Heed and Wingård tested their converter by using them on six natural gas fueled trucks. During the test period the trucks were in ordinary use; driving around in the area of Gothenburg at low engine loads. The result for one day is shown in Figure 1.

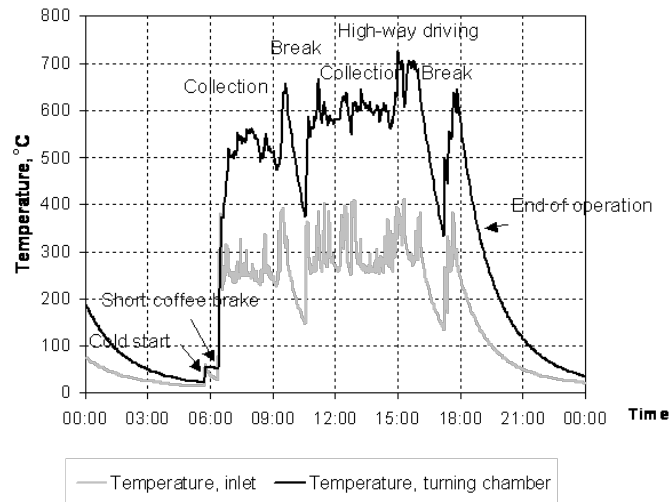


Figure 1: The heat exchanger implemented on a truck driving in Gothenburg [5].

As the trucks starts the inlet temperature rises, and after a while the light off temperature is reached which leads to a significant temperature increase at the catalyst. The temperature stays quite high during the whole day, including lunch and other pauses. The fact that there is a temperature difference is proof that reactions occur at the catalyst. The trucks were also subjected to a standardized exhaust gas test. In Figure 2 the results from long time tests are shown, it can be seen that the conversion efficiency is settling towards 70%. [5]

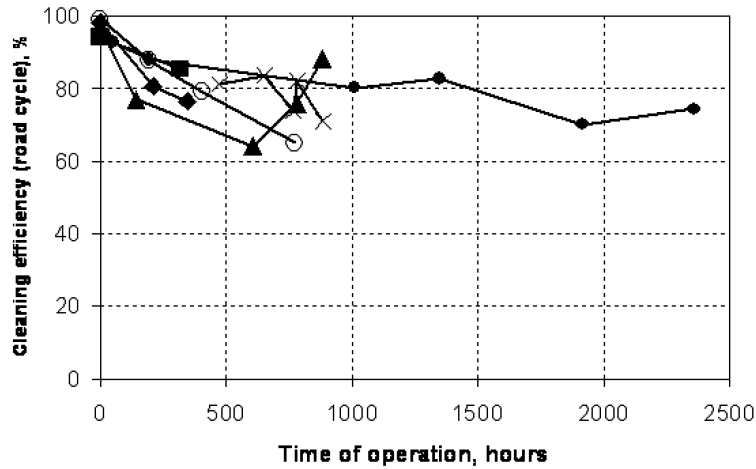


Figure 2: The effect of catalyst aging [5].

## 2.2 Integrated and Sequential Heat Exchangers

According to a study performed by Rink et al., a transient 1-D simulation of a cold start was simulated with ProMot/DIANA, it was concluded that the time it took for the catalyst to be heated up was too long in order for it to be considered acceptable [4]. It was hence concluded that some kind of additional heating was required in order to reduce the emissions during a cold start. In another study performed by Rink et al., three different design concepts consisting of heat exchangers, burners and catalysts in the after treatment system for a diesel engine were simulated [6]. The first constellation consisted of a diesel oxidation catalyst (DOC), where the inflow gas was at the same temperature as the gas output of the engine. A second system was constructed with a fuel boiler added to the system. The fuel boiler was placed between the engine and the DOC, as shown in Figure 3a, heating the gas inflow of the DOC. The third constellation consisted of a DOC, a fuel boiler and a folded sheet-type heat exchanger. The heat exchanger was placed between the engine and the fuel boiler which, as in the previous case, was placed before the DOC as shown in Figure 3b.

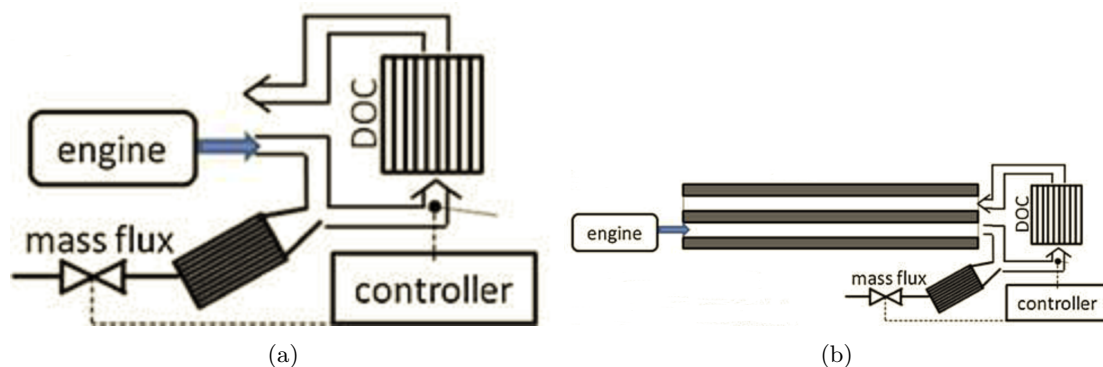


Figure 3: Schematics of (a) the fuel boiler and the DOC and (b), the heat exchanger, the fuel boiler and the DOC [6].

All Three concepts were then simulated with a 1-D model which took into account the variation of temperature, pressure and mass fraction of the species included in the model. The simulations results regarding the temperature of the DOC are presented in Figure 4.

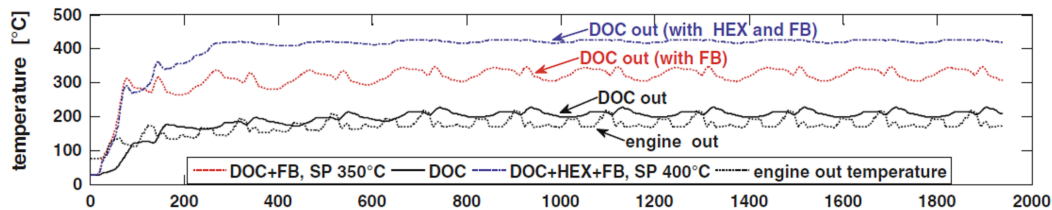


Figure 4: The output temperature [6].

It became clear that the highest outlet temperature of the DOC was reached in the case where both heat exchanger and a fuel boiler were present. It is also concluded that the outlet temperature from the DOC was rather identical during the startup, since the heat exchanger needed time to be heated up before providing additional heat to the DOC. However, by adding the fuel boiler, disturbance of the exhaust air fuel-ratio was detected, which is important for optimum catalyst performance. In addition, a significant increase in the cost for the heat exchanger system would have to be expected with the added boiler.

Rink et al., introduced another way to solve the problem with cold start; the use of an electric heater that is closely attached to the catalyst [4]. The idea is that the electric heater will be used during cold start until a high enough temperature is reached, such that the catalyst temperature can be maintained by the heat exchanger. In order to quickly heat the system a bypass option was introduced, shown in Figure 5. During cold start a flap is opened such that the exhaust gas flows through the electric heater directly into the catalyst coated outflow channels. Soon a high enough temperature will be reached in the catalyst such that conversion of the pollutants will start, which will further increase the heating of the catalyst. Once sufficiently high temperature has been reached the flap will close and normal counter current mode will be used, i.e. the exhaust gas enters the heat exchanger from the side channel and will be preheated by the hot exhaust gas from the outflow channels. An additional advantage with this system is that during a high load period when the temperature out from the engine already is high the flap can be opened but without turning on the electric heater. This allows the exhaust gas to enter the catalyst without first being preheated, and hence too high temperatures in the catalyst can be avoided [4].

In order to test this system, Rink et al., used a vacuum-brazed stainless steel parallel plate-type heat exchanger with a cross section of 5 times 8cm and a total length of 30cm and with a coated length of 10cm [7]. As coating a mixture of  $Pd/Rh$  was used. The feed gas had a temperature of 180°C, a flow rate of 9m<sup>3</sup>/h and the power output of the electric heater was 1 kW. The gas composition consisted of 0.5%  $CO$  and 3,500 ppm  $CH_4$ . This experimental setup gave the results shown in Figure 6.

In Figure 6a the inflow temperature is defined as the temperature after the electric heater. In Figure 6b the result of this experimental setup shows that it is possible to reach good conversion. However this system has a few drawbacks, the large thermal mass of the metallic heat exchanger means that quite some time is needed during cold start before normal operation mode can be entered. As shown in Figure 6, when the inflow temperature is compared to the catalyst

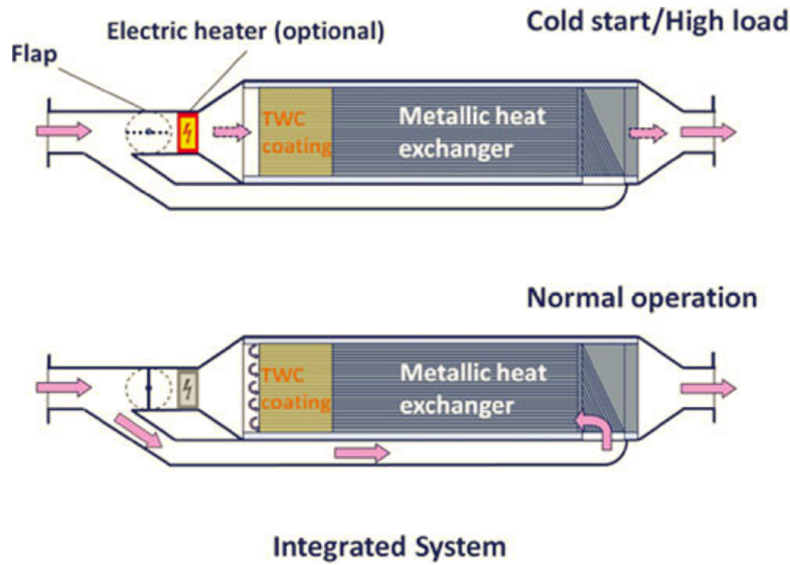


Figure 5: Heat exchanger with electric heater and a bypass [4].

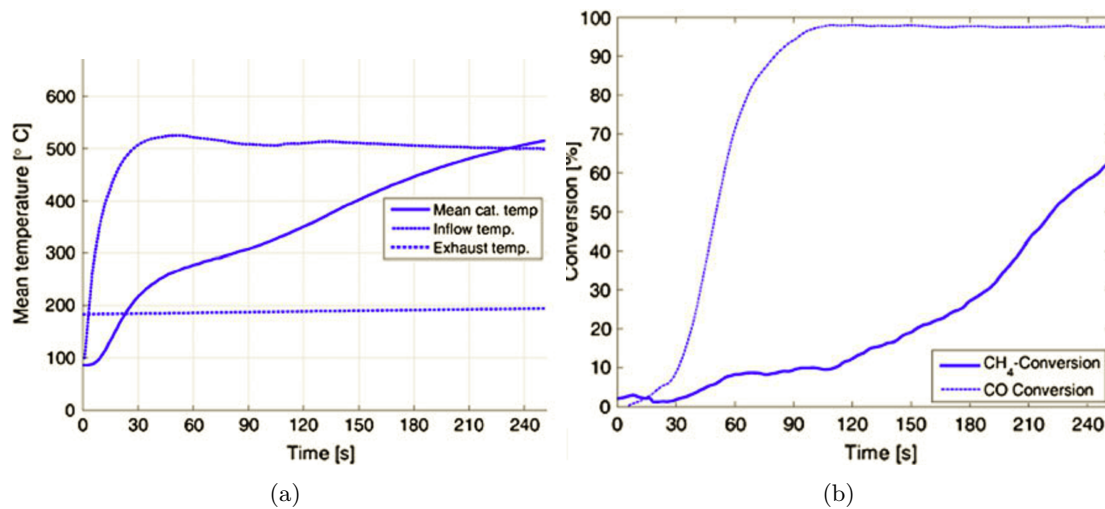


Figure 6: Experimental results from the prototype (a) temperature (b) conversion [7].

temperature, it can be seen that the large thermal mass of the system results in slow heating of the system. Due to back pressure and manufacturing constraints the heat exchanger channels have much larger dimensions than normally used in catalysis. During cold start only the outflow channels are used which mean that only half of the available catalyst area is passed, i.e. less conversion of the pollutants. Due to these drawbacks, Rink, et. al, introduced a sequential concept where a ceramic monolith catalyst is combined with a metallic heat exchanger [7]. This concept is shown in Figure 7. The idea is that lower thermal mass and larger catalytic area will decrease the time needed for the system to get heated after cold start. With this system high cell density can be used in the catalyst while the heat exchanger can have larger dimensions in order to minimize the pressure drop. Moreover at cold start, the flap will open and the exhaust gas will

pass the entire catalyst area. Once sufficient temperature has been reached, the flap will close, and the exhaust gas will enter the counter current heat exchanger. After the heat exchanger the gas needs to go through another side channel such that the gas can enter the catalyst. This side channel will at first be cold, leading to a temperature drop. This effect can be compensated by extending the initial heating period.

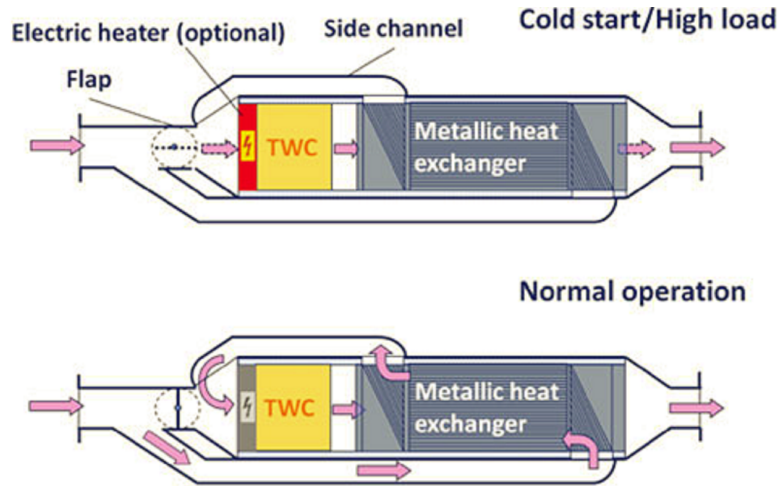


Figure 7: A sequential layout with separated catalyst and heat exchanger [7].

In order to compare the integrated system with the sequential system, Rink et al., used a 1D model that they implemented in PROMoT/DIANA [7]. For the integrated system the length of the heat exchanger is  $0.3m$  out of which  $0.1m$  is coated. The length of the heat exchanger in the sequential system is  $0.2m$ . The result of the temperatures for the integrated system and the serial system are shown in Figure 8 and the result of accumulated methane for both the systems are shown in Figure 9.

The electric heater is turned on for the first  $80s$ , which gives rapid heating of the exhaust gas, the dotted line, and later the decrease at the  $80s$  mark. The solid line represents the mean temperature in the catalyst. It can be seen that the gradient of the mean catalyst temperature is steeper for the serial system; this is due to the lower thermal mass. The accumulated methane is at first much lower for the sequential system since the temperature is rising faster, but once the flap is closed there is an increase of methane since the cold side channel decreases the temperature. This effect could however be limited if the electric heater was on for a longer period or if the side channel somehow was preheated [7].

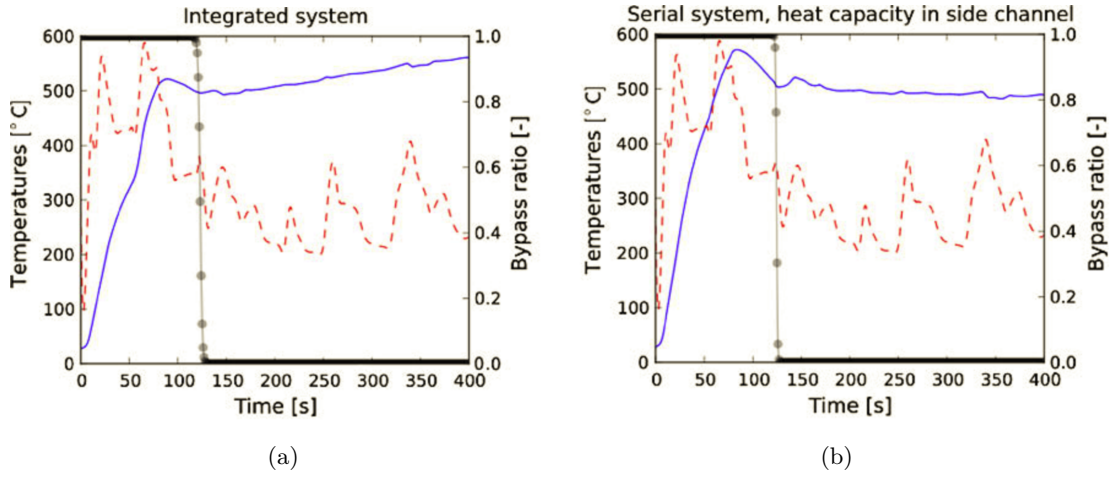


Figure 8: Modeling results comparing the temperature (a) integrated system (b) sequential system [7].

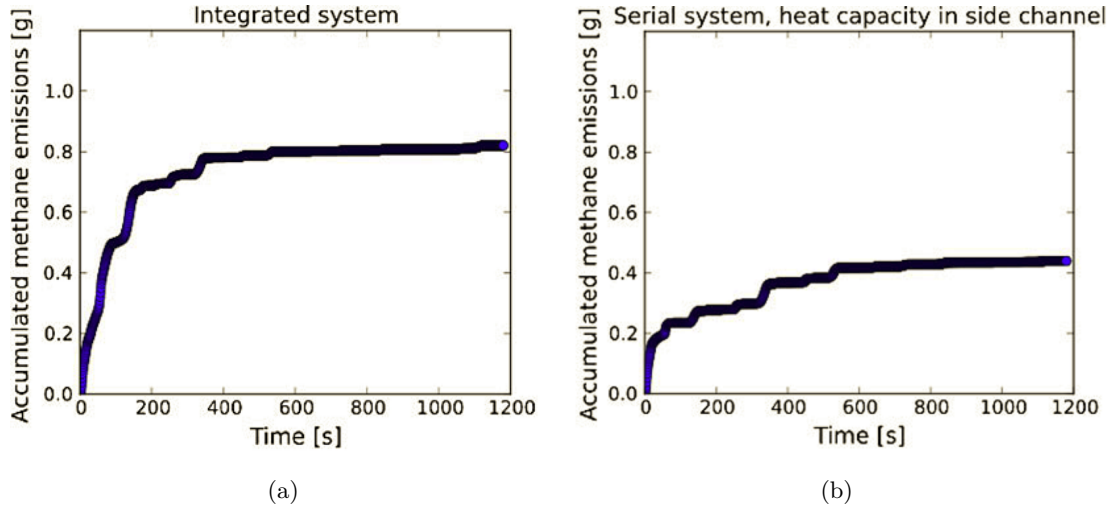


Figure 9: Modeling results comparing the conversion (a) integrated system (b) sequential system [7].

### 3 Theory and Simulation Methods

The theory section starts by giving an introduction to heat exchangers and some of the correlations that are used to calculate the performance of a heat exchanger. A mathematical model that describes the transient behavior of a heat exchanger will be developed. Finally the theory behind CFD will be introduced, such that the results of the computational fluid dynamics can be used to find performance parameters of a heat exchanger, based on any arbitrary geometry.

### 3.1 Heat Exchangers

Several different types of heat exchangers exist, e.g. shell and tube heat exchangers, plate heat exchangers and spiral heat exchangers. The heat exchanger has to occupy a very small volume, in order for it to fit in the truck. Hence the idea is to implement a plate heat exchanger, which has the advantage that a very large surface area can be formed in a small volume, and that the overall heat transfer coefficient is relatively high - up to five times larger than the coefficient of shell and tube heat exchangers. A disadvantage is however that the pressure drop may be relatively high and that there is a possibility of leakage. The heat exchanger is formed by pressing the plates together, but to avoid leakage problems plate exchangers are mainly used for liquids. There are however brazed constructions that allow plate heat exchangers to be used for gas-to-gas applications. A schematic view of how a plate heat exchanger works is shown in Figure 10a.

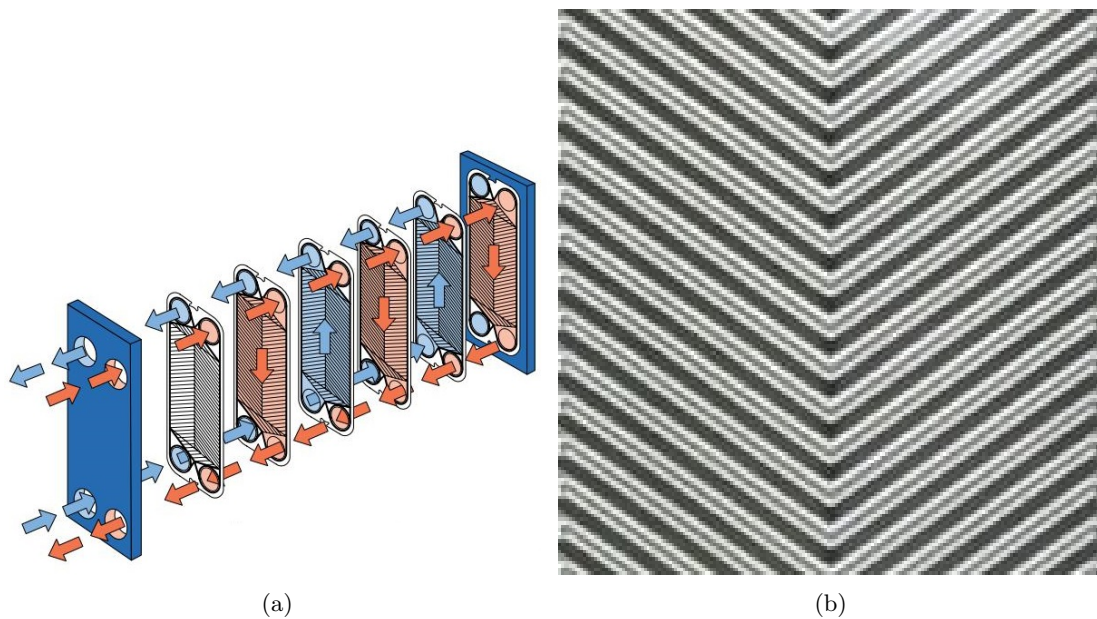


Figure 10: Schematic overview over (a) a plate heat exchanger (b) a Chevron plate.

The heat transfer is heavily dependent on the design of the plates, which are corrugated in order to increase the surface area and to enhance turbulence. One typical design is the so called Chevron, or herringbone, corrugations[8], which can be shown in Figure 10b. The Chevron angle is defined as the angle between the mid-section of the plate and the corrugations.

#### 3.1.1 Plate Heat Exchanger Corrugations

Corrugations are implemented upon a plate heat exchangers to improve the heat transfer. The increase in heat transfer for a herringbone shaped heat exchanger is mainly due to that a larger heat transfer area is present due to the corrugations and the occurrence of separation and reattachment of the boundary layers of the fluid as well as vortex and swirl generation created in the fluid. In addition to an increased heat transfer, the friction coefficient is also increased for corrugated plates, thereby also increasing the pressure drop for the corrugated plate heat exchanger [9].

There are several different corrugation patterns available on the market today, were the herringbone (V-shaped) pattern is one of the most common. The corrugations in the herringbone pattern is creating channels which meets up in the center of the plate. These channels direct the flow towards the middle of the plate where the flow then is forced to pass the corrugations, creating swirls and breaking the boundary layer of the fluid. Different shapes and geometries of the corrugations therefore creates different flow patterns, indicating that the geometrical setup is of great importance. Under or over-sizing of the heat exchanger often leads to flow maldistribution and large temperature differences as well as an uncertainty of the pressure drop.

A common shape of the corrugations are a rounded sine waved shape, but shapes of triangles and plateaus are also existing. However, studies have shown that that actual shape of the corrugations matters little since the Nusselt numbers, given a fixed Reynolds number and Chevron angle for the different shapes included in the study (trapezoidal, triangular and sinusoidal), differed very little. The pressure drop does however vary significantly between the cases, from which the sinusoidal shaped corrugations produced the smallest and the triangular shaped the largest pressure drop [9].

The height and width of the corrugations are also of importance. A high aspect ratio (corrugation height divided by corrugation width) is desirable for high heat transfer, since it creates additional swirls in the flow which improves the heat transfer by reducing the heat transfer resistance in the boundary layer. The drawback is however that it also increases the pressure drop for the system [10].

### 3.1.2 Chevron Angles

The Chevron angle refers to the inclined angle for which the flow approach the corrugation. The adjacent plates have corrugations where the incline is reversed, so that when the heat exchanger is assembled the path of the fluid involves several changes in direction and has a cross section that varies [11].

In a flow visualization study by Focke et al., the flow patterns for different Chevron angles given fixed Reynolds numbers were presented [11]. In Figure 11, the flow patterns for two different angles from this study is presented.

As shown in Figure 11, the flow patterns differ greatly. In the case with lower Chevron angles the flow follows the corrugation channels until it reaches the walls of the heat exchanger. At the wall it is forced to turn and enters the corrugation channel in the opposite plate which it follows until the next wall were the process is repeated. In the case were the Chevron angles are 80 degrees, the flow pattern is completely different. The flow follows the corrugations channels to some extent, but is after a short distance forced to switch into the corrugation channel of the opposite plate, which it follows for a while in a seemingly repeating pattern. The switches occurs due to the swirls of the flow within the corrugation channels, created by the sharp Chevron angles.

In another study performed by Focke et al., heat transfer and pressure drop were analyzed for different Chevron angles [12]. An interesting result from this study is how the heat transfer and the pressure drop changed when altering the Chevron angles, for fixed Reynolds numbers. The result is presented in the Figure 12.

As shown in Figure 12, the Chevron angle have a large effect upon both the heat transfer and the pressure drop. It should however be noted that the pressure drop is increasing rapidly for high Chevron angles. By comparing the Chevron angles of 30° and 60° for the case with  $Re = 500$ ,

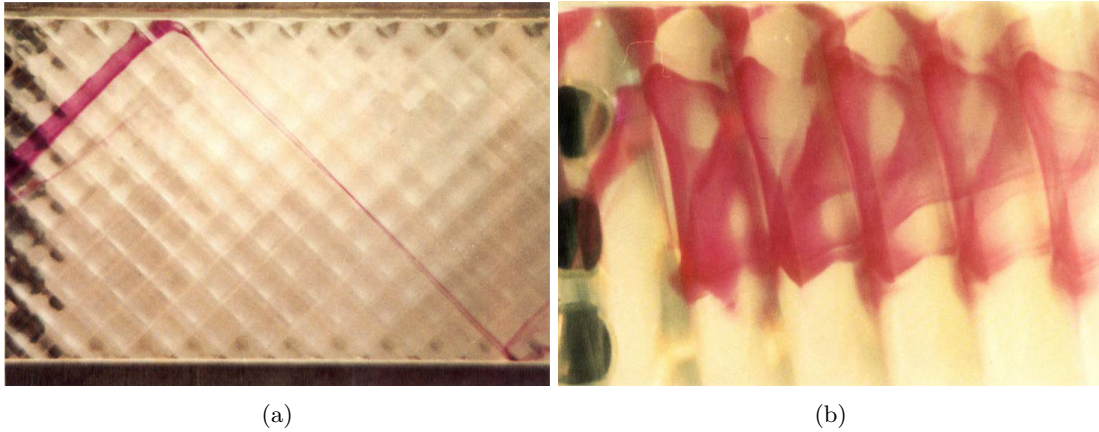


Figure 11: Flow patterns (a) Chevron angles at 45 degrees with a Reynolds number of 70 (b) Chevron angles at 80 degrees at a Reynolds number of 80 [11]

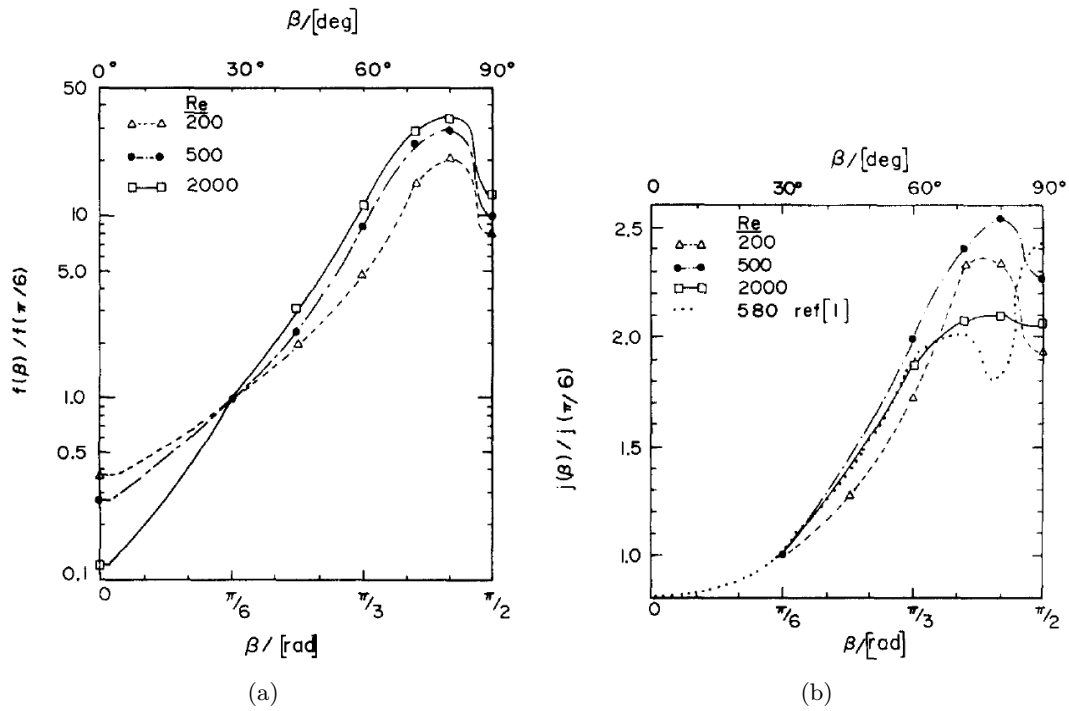


Figure 12: The effect of the corrugation inclination angle for fixed Reynolds numbers for (a) the pressure drop (b) heat transfer [12].

one can see that the heat transfer has doubled for the 60° case while the pressure drop has increased tenfold. Further on, a heat transfer maximum is reached when the inclination angle of the flow is at roughly 80°, which also produces the highest pressure drop. The cases with a Chevron angle between 30 – 60° are assumed to have a similar flow pattern as the 45° case presented in Figure 11. The difference within these flow are the swirling motions within the

corrugation channels, created by crossing streams. The swirling motion is generated by the flow in the opposite corrugation channel. For Chevron angles less than  $45^\circ$ , the velocity component of both channels are positive since they have a flow velocity in the direction of the stream. For inclination angles larger than 45 degrees this effect is instead negative which, according to Focke et al., might be the reason to the change of flow patterns observed at a Chevron angle of  $80^\circ$ .

The dotted line in the left figure 12b refers to a study performed by Rosenblad and Kullendorff, does however disagree with the results gathered by Focke et al., and actually have a local minimum at the inclination angle of  $80^\circ$  and instead have their maximum heat transfer at an inclination angle of  $72^\circ$  [12]. Both experiments were carried out with sinusoidal corrugation patterns with a pitch of  $10\text{mm}$ , but different amplitudes of the height of the corrugations. The heights were  $2.5\text{mm}$  and  $1.6\text{mm}$  in studies performed by Focke et al. and Rosenblad/Kullendorff respectively, which might be a possible explanation of the differences. An alternative theory presented by Focke et al. is that the corrugation on the Rosenblad and Kullendorff study might have been out of phase at high inclinations angles.

### 3.1.3 Flow Properties

Another important aspect for the flow profiles and heat transfer in the plate heat exchanger is the properties of the flow. For very low Reynolds numbers, the flow is laminar. As the Reynolds number increases turbulent tendencies appears and vortexes are created which enhances the heat transfer but also increases the pressure drop. Further, higher Reynolds numbers also forces the homogeneity of the flow to increase which is desirable in order to achieve a more uniform flow profile through out the heat exchanger, resulting in higher heat transfer [13].

An important observation is that the factors that increases the heat transfer within the heat exchanger also tend to increase the pressure drop. It is therefore often the accepted pressure drop of the system that limits the potential heat transfer rate of the heat exchanger and thereby also its design.

### 3.1.4 Correlations

The total heat transfer in a plate heat exchanger can be written as

$$Q = UA\Delta\theta_M. \quad (1)$$

Where  $U$  is the overall heat transfer coefficient,  $A$  is the total plate area and  $\Delta\theta_M$  is the effective temperature difference. It is important how  $A$  is defined, as it may be either defined as the true surface area, including the corrugations, or as the projected area. The correlations used to calculate the heat transfer coefficients must be based on the same area. The overall heat transfer coefficient can be calculated from,

$$\frac{1}{U} = \frac{1}{h_h} + \frac{1}{h_c} + \frac{d_p}{k_p} + R_f. \quad (2)$$

Where  $h$  is the convective heat transfer coefficient,  $d_p$  is the thickness of the plates,  $k_p$  is the conductivity of the plates and  $R_f$  represents the fouling resistance for the plate. The convective heat transfer coefficient is dependent on the fluid properties, the velocity of the fluid and the plate geometry.  $h$  is often calculated by experimentally obtained correlations. The correlations are specific for each plate design and are often only known by the manufacturers. The correlations are often in the form,

$$Nu = a(Pr)^b(Re)^c \quad (3)$$

Where  $Nu$ ,  $Pr$  and  $Re$  are the dimensionless numbers defined by,

$$\begin{aligned} Nu &= \frac{hD_e}{k} \\ Pr &= \frac{c_p\mu}{k} \\ Re &= \frac{vD_e\rho}{\mu}, \end{aligned} \quad (4)$$

and the constants  $a, b$  and  $c$  are dependent on the specific geometry and the Reynold number. As an example for a plate with a chevron angle of  $30^\circ$  and a flow situation with Reynold around 1000 – 10000, the area of the plate defined as the projected area and with the material properties evaluated at the mean bulk temperature, the correlation may be written,

$$Nu = 0.4(Pr)^{0.4}(Re)^{0.64}. \quad (5)$$

For this case the friction factor,  $f$ , may be calculated from,

$$f = 2.78Re^{-0.18} \quad (6)$$

and hence the pressure drop over the plate can be calculated as[8],

$$\Delta p = 4f \frac{L}{D_e} \frac{\rho v^2}{2}. \quad (7)$$

In order to get the total pressure drop over the heat exchanger there should be an addition for the pressure drop over the in and outlet.

In order to evaluate the heat exchanger, the thermal effectiveness is how close the actual heat transfer is compared to the maximum possible heat transfer. The effectiveness will be 1 if the cold outlet temperature reaches the hot inlet temperature, which happens if the heat exchanger has infinite area or infinite convective heat transfer [15]. Hence the the equations for the effectiveness can be written as,

$$E = \frac{\dot{m}_c C_{p_c} (\theta_{c_{out}} - \theta_{c_{in}})}{\dot{m}_h C_{p_h} (\theta_{h_{in}} - \theta_{c_{in}})}. \quad (8)$$

### 3.1.5 Steady State Model

To get an understanding of what temperatures the heat exchanger may reach under typical conditions a simple steady state model was developed. For this model it will be assumed that the heat exchangers has plates with a chevron angle of  $30^\circ$ , i.e such that the above correlation can be used. To get the temperature out from the heat exchanger the following three equivalent expressions for the total heat transfer are used [8],

$$\begin{aligned} Q &= \dot{m}_c C_{p_c} (\theta_{c_{out}} - \theta_{c_{in}}) \\ Q &= \dot{m}_h C_{p_h} (\theta_{h_{in}} - \theta_{h_{out}}) \\ Q &= UA\Delta\theta_M. \end{aligned} \quad (9)$$

The mass flow that enters the cold side of the heat exchanger will go through the catalyst and then enter the hot side, i.e.  $\dot{m}_c = \dot{m}_h$ . The heat capacity will change in the heat exchanger as the

temperature is changing, but just as in the case of the correlation for the heat transfer coefficient, the heat capacity will be evaluated at the mean bulk temperature. However there will be a change of species, methane will react with oxygen and give carbon dioxide and water, which will have an impact on the heat capacity. However the flow will be approximately 99.8% air and 0.2% methane and it will hence be assumed that the heat capacity will be the same for the cold and hot flow. This gives that  $(\theta_{c_{out}} - \theta_{c_{in}}) = (\theta_{h_{in}} - \theta_{h_{out}})$ , i.e  $(\theta_{h_{in}} - \theta_{c_{out}}) = (\theta_{h_{out}} - \theta_{c_{in}}) = \Delta\theta$ . Hence the effective temperature difference  $\Delta\theta_M$  will be equal to  $\Delta\theta$ . Using this in equations 9 gives  $UA(\theta_{h_{in}} - \theta_{c_{out}}) = \dot{m}C_p(\theta_{c_{out}} - \theta_{c_{in}})$ . Where  $\theta_{h_{in}}$  can be expressed as  $\theta_{h_{in}} = \theta_{c_{out}} + \Delta\theta_{reac}$ , and the increase of temperature can be calculated from the percentage of methane assuming that everything will react. A balance over the reaction gives that  $\Delta H_r \dot{m}y = C_p \dot{m} \Delta\theta_{reac}$ , where  $\Delta H_r$  is reaction enthalpy for combustion of methane and  $y$  is the percentage of methane. Combining these expressions gives that the temperature into the catalyst, once steady state is reached, will be

$$\theta_{c_{out}} = \frac{\left(\frac{UA\Delta H_r y}{c_p} + \dot{m}C_p\theta_{c_{in}}\right)}{\dot{m}C_p}. \quad (10)$$

Hence given the total mass flow, the inlet temperature, the percentage of methane and number of plates, the temperature into the catalyst can be calculated. The number of channels will give the mass flow and the velocity for each channel, assuming a uniform velocity profile and that the fluid is distributed equally between the channels. Hence the Reynold number can be calculated, and correlations 5 and 6 can be used to calculate the convective heat transfer coefficient and the pressure drop. Equation 2 is used to obtain the overall heat transfer coefficient, which enables the use of equation 10.

### 3.2 Transient Response of a heat exchanger

The steady state model only gives information about what the temperature into the catalyst will be for fixed values of the mass flow, inlet temperature and percentage of methane. Since these variables are constantly changing it is important to get an understanding of how the heat exchanger responds when these variables are changing. Hence a mathematical model for a plate heat exchanger will be developed. The literature available in the area of thermal simulation of plate heat exchangers is vast. The transient response for multi-pass plate heat exchangers including the effect of axial thermal dispersion in the fluid was presented by S.K. Das and K. Murugesan [16], the dynamics of plate heat exchangers subject to flow variations was presented by A.K. Dwivedi and S.K. Das [17], and the transient response of plate heat exchangers considering the effect of flow maldistribution was presented by N. Srihari et al. [18]. The model that will be developed in this thesis will be built upon these three articles but with a few extra simplifications. The assumptions that are needed to develop the model are:

- All flow and thermal properties of the fluids are considered to be independent of the temperature.
- Heat transfer takes place only across the plates and not through the seals.
- The heat exchanger is thermally insulated from heat leak to the surroundings.
- Thermal conductance is infinite across the thickness of the plate but negligible along the length of the plate.
- The fluid back-mixing in the flow passages is neglected.
- The axial dispersion of the fluid within the channels is neglected.

- The flow distribution inside the channels is taken as "plug flow", i.e. uniform flow.
- The projected area of the plate is taken as heat transfer area.
- The flow maldistribution from channel to channel is neglected, instead it is considered that the flow divides evenly between the channels.
- The heat transfer coefficient is considered to be a function of fluid velocity in respective channel, i.e for an even amount of channels with the flow dividing evenly the heat transfer coefficient will be the same for each channel.

The cold fluid will flow in channels 1,3,5...N-1 and will be denoted 1, the hot fluid will flow in the even channels 2,4,6...N and will be denoted 2. Where the total number of channels, N, is chosen to be even. The coordinate system is chosen to be in the direction of the cold fluid.

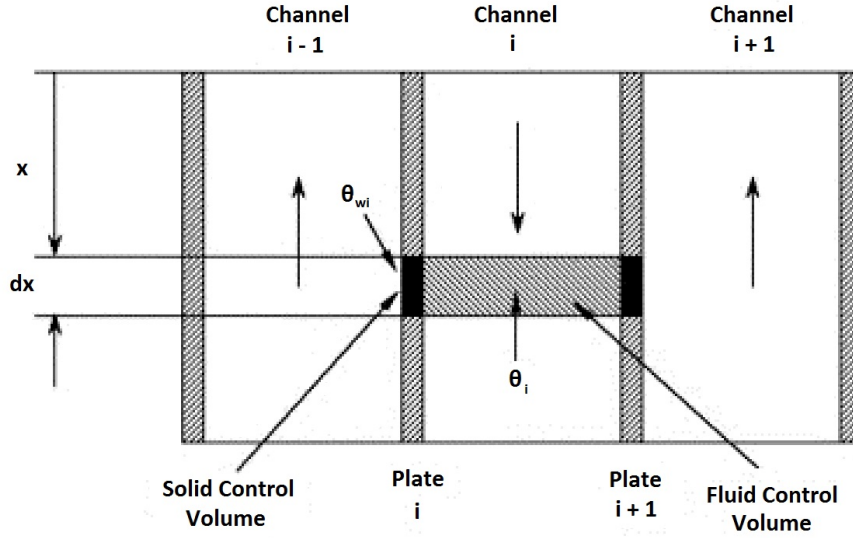


Figure 13: Control volumes over the fluids and plates.

Small elements of fluids and plate can be considered as control volumes, which can be seen in Figure 13, by applying the energy equation to the control volumes considering the above assumptions, the equations becomes for the cold fluid:

$$\frac{C_1}{L} \frac{\partial \theta_i}{\partial \tau} = -(-1)^{i-1} \dot{m}_i C_{p_i} \frac{\partial \theta_i}{\partial x} + \frac{h_i A}{2L} (\theta_{wi} + \theta_{wi+1} - 2\theta_i) \quad i = 1, 3, 5 \dots N - 1 \quad (11)$$

hot fluid:

$$\frac{C_2}{L} \frac{\partial \theta_i}{\partial \tau} = -(-1)^{i-1} \dot{m}_i C_{p_i} \frac{\partial \theta_i}{\partial x} + \frac{h_i A}{2L} (\theta_{wi} + \theta_{wi+1} - 2\theta_i) \quad i = 2, 4, 6 \dots N \quad (12)$$

for plates 2 to N:

$$\frac{C_w}{L} \frac{\partial \theta_{wi}}{\partial \tau} = \frac{h_{i-1} A}{2L} (\theta_{i-1} - \theta_{wi}) + \frac{h_i A}{2L} (\theta_i - \theta_{wi}) \quad i = 2, 4, 6 \dots N \quad (13)$$

for end plate 1:

$$\frac{C_w}{L} \frac{\partial \theta_{w1}}{\partial \tau} = \frac{h_1 A}{2L} (\theta_1 - \theta_{w1}) \quad (14)$$

for end plate  $N + 1$

$$\frac{C_w}{L} \frac{\partial \theta_{w,N+1}}{\partial \tau} = \frac{h_2 A}{2L} (\theta_N - \theta_{w,N+1}) \quad (15)$$

Where  $C_i$  is the heat capacity for respective resident fluid and  $C_w$  is the heat capacity of the wall, defined by  $C_i = C_{p_i} \rho_i A_c L$  and  $C_w = C_{p_p} \rho_p A_p d_p$ .  $A_c$  is the free flow area of the channel,  $A_p$  is the area of the plates and  $d$  is the thickness of the plates. The equations can be written in dimensionless form by,

$$\begin{aligned} X = \frac{x}{L} \quad T = \frac{\theta - \theta_{1,in}}{\theta_{2,in} - \theta_{1,in}} \quad t = \frac{\tau}{\tau_r} \\ U_i = \frac{h_i A}{\dot{m} c_p} \quad R_c = \frac{C_w}{C_1} \end{aligned} \quad (16)$$

where  $\tau_r = \frac{C}{\dot{m} c_p}$ . Using the same assumption as in the steady state model, i.e. the properties are the same for the hot and cold fluids, the equation for the fluid becomes,

$$\frac{\partial T_i}{\partial t} = -(-1)^{i-1} \frac{\partial T_i}{\partial X} + \frac{U}{2} (T_{wi} + T_{w,i+1} - 2T_i) \quad i = 1, 2, 3, 4, \dots, N. \quad (17)$$

For plates 2 to N:

$$R_c \frac{\partial T_{wi}}{\partial t} = \frac{U}{2} (T_{i-1} - T_{wi}) + \frac{U}{2} (T_i - T_{wi}) \quad i = 2, 4, 6, \dots, N \quad (18)$$

For the first plate:

$$R_c \frac{\partial T_{w1}}{\partial t} = \frac{U}{2} (T_1 - T_{w1}) \quad (19)$$

For the last plate:

$$R_c \frac{\partial T_{w,N+1}}{\partial t} = \frac{U}{2} (T_N - T_{w,N+1}) \quad (20)$$

These equations are hence to be solved in order to get an understanding of the transient response for the heat exchanger.

### 3.2.1 Boundary Conditions

For the above governing equations, the boundary conditions can be set as,

$$\begin{aligned} \text{at } X = 0 \quad T_i = 0 \quad \text{for } i = 1, 3, 5, \dots, N - 1 \\ \text{at } X = 1 \quad T_i = 1 \quad \text{for } i = 2, 4, 6, \dots, N \end{aligned} \quad (21)$$

Hence for the cold fluid at  $x = 0$  the temperature will be  $\theta = \theta_{1,in}$  and for the hot fluid at  $x = L$  the temperature will be  $\theta = \theta_{2,in}$ . One of the goals is to investigate how the heat exchanger

responds when the the inlet temperature of the cold stream and/or the inlet temperature of the hot stream changes. This may be expressed in the boundary conditions as,

$$\begin{aligned} \text{at } X = 0 \quad T_i &= 0 + aH(t - t_0) \quad \text{for } i = 1,3,5,\dots,N - 1 \\ \text{at } X = 1 \quad T_i &= 1 + bH(t - t_0) \quad \text{for } i = 2,4,6,\dots,N \end{aligned} \quad (22)$$

Where H is the Heaviside function defined by  $H(t - t_0) = 1$  for  $t > t_0$  and  $H(t - t_0) = 0$  for  $t < t_0$ .  $a, b$  represents the size of the changes to the temperatures. Several Heaviside functions may be added to the boundary conditions, in order to simulate several temperature changes.

### 3.2.2 Solution Procedure

To solve the system of partial differential equations the idea is to use Laplace transform with respect to the time variable, i.e.  $T(t, X) \rightarrow \hat{T}(s, X)$ , which is defined by  $\hat{T}(s, X) = \int_0^\infty T(s, X)e^{-st}dt$ . Using the definition of the Laplace transform allows the equations to be written as,

$$\begin{aligned} (-1)^{i-1} \frac{d\hat{T}_i}{dX} &= -s\hat{T}_i - T_i(0, X) + \frac{U}{2}(\hat{T}_{wi} + \hat{T}_{w,i+1} - 2\hat{T}_i) \\ & \quad i = 1,2,3,4,\dots,N \end{aligned} \quad (23)$$

For plates 2 to N:

$$\begin{aligned} s\hat{T}_{wi} - T_{wi}(0, X) &= \frac{U}{2R_c}(\hat{T}_{i-1} - \hat{T}_{wi}) + \frac{U}{2}(\hat{T}_i - \hat{T}_{wi}) \\ & \quad i = 2,4,6,\dots,N \end{aligned} \quad (24)$$

For the first plate:

$$s\hat{T}_{w1} - T_{w1}(0, X) = \frac{U}{2R_c}(\hat{T}_1 - \hat{T}_{w1}) \quad (25)$$

For the last plate:

$$s\hat{T}_{w,N+1} - T_{w,N+1}(0, X) = \frac{U}{2R_c}(\hat{T}_N - \hat{T}_{w,N+1}) \quad (26)$$

Where the initial temperature for the fluid and the wall may be set to zero,  $T_i(0, X) = 0$   $T_w(0, X) = 0$ , i.e the same as the inlet temperature. It should be noted that that it is possible to set this value to something else than zero. This has been attempted and it leads to some particular solutions that are not to hard to calculate by hand, but was hard to implement in the code. By substituting equations 24, 25, 26 into equation Eq. 23, it reduces to the final single equation,

$$\frac{d\hat{T}_i}{dX} = (-1)^{i-1} \left( \hat{T}_i \left( -s - U + \frac{U^2}{4(sR_c + k_i + k_{i-1})} + \frac{U^2}{4(sR_c + k_i + k_{i+1})} \right) \right) \quad (27)$$

$$\begin{aligned} & + \hat{T}_{i-1} \left( \frac{U^2}{4(sR_c + k_i + k_{i-1})} \right) + \hat{T}_{i+1} \left( \frac{U^2}{4(sR_c + k_i + k_{i+1})} \right) \\ & \quad i = 1,2,3,4,\dots,N \end{aligned} \quad (28)$$

where  $k_i = \frac{U}{2}$  and is given the index in order to implement that  $k_0 = 0$  and  $k_{N+1} = 0$ . It can also be noted that  $T_0 = 0$  and  $T_{N+1} = 0$ . Similarly the boundary conditions, Eq.22, can be transformed into,

$$\begin{aligned} \text{at } X = 0 \quad T_i &= 0 + \frac{ae^{-t_0s}}{s} \quad \text{for } i = 1,3,5,\dots,N - 1 \\ \text{at } X = 1 \quad T_i &= \frac{1}{s} + \frac{ae^{-t_0s}}{s} \quad \text{for } i = 2,4,6,\dots,N \end{aligned} \quad (29)$$

The transformed Eq., 28, can be expressed in matrix form as

$$\frac{d\bar{T}}{dX} = \bar{A}\bar{T} \quad (30)$$

where,

$$\begin{aligned} \bar{A}_{i,i} &= (-1)^{i-1} \left( -s - U + \frac{U^2}{4(sR_c + k_i + k_{i-1})} + \frac{U^2}{4(sR_c + k_i + k_{i+1})} \right) \\ \bar{A}_{i,i-1} &= (-1)^{i-1} \left( \frac{U^2}{4(sR_c + k_i + k_{i-1})} \right) \\ \bar{A}_{i,i+1} &= (-1)^{i-1} \left( \frac{U^2}{4(sR_c + k_i + k_{i+1})} \right), \end{aligned} \quad (31)$$

and the rest of the entries in the matrix are zero. This is a simple boundary value problem with the distance coordinate, X, as the only variable. The solution is given by

$$\begin{aligned} \hat{T}_i &= \sum_{j=1}^N d_j u_{ij} e^{\beta_j X} \\ i &= 1, 2, 3, \dots, N \end{aligned} \quad (32)$$

where  $\beta_j$  are the eigenvalues of the matrix  $\bar{A}$  and the  $u_j$  are the corresponding eigenvectors. The coefficients  $d_j$  are determined by the boundary conditions, 29, and the equations for the coefficients becomes

$$\begin{aligned} \sum_{j=1}^N d_j u_{ij} &= 0 + \frac{ae^{-t_0 s}}{s} \quad \text{for } i = 1, 3, 5, \dots, N-1 \\ \sum_{j=1}^N d_j u_{ij} e^{\beta_j} &= \frac{1}{s} + \frac{ae^{-t_0 s}}{s} \quad \text{for } i = 2, 4, 6, \dots, N \end{aligned} \quad (33)$$

The boundary conditions will form the vector  $K$ , and  $u_{ij}$  and  $u_{ij}e^{\beta_j}$  will form the matrix  $B$  such that the following equation system will be obtained,

$$\begin{pmatrix} u_{11} & \cdots & u_{1N} \\ u_{21}e^{\beta_1} & \cdots & u_{2N}e^{\beta_N} \\ u_{31} & \cdots & u_{3N} \\ \cdots & \cdots & \cdots \\ u_{N1}e^{\beta_1} & \cdots & u_{NN}e^{\beta_N} \end{pmatrix} \times \begin{pmatrix} d_1 \\ d_2 \\ d_3 \\ \cdots \\ d_N \\ d \end{pmatrix} = \begin{pmatrix} 0 + \frac{ae^{-t_0 s}}{s} + \cdots \\ \frac{1}{s} + \frac{be^{-t_0 s}}{s} + \cdots \\ 0 + \frac{ae^{-t_0 s}}{s} + \cdots \\ \cdots \\ \frac{1}{s} + \frac{be^{-t_0 s}}{s} + \cdots \end{pmatrix}. \quad (34)$$

This allows the coefficients to be obtained from,

$$d = B^{-1}K. \quad (35)$$

### 3.2.3 Modeling the Catalyst

Instead of setting a temperature at the inlet to the hot side of the heat exchanger, the model is improved by adding a model for the catalyst. The idea is that the outlet flow from the cold side of the heat exchanger will enter the catalyst, where the methane will react and therefore give an increase in temperature to the hot side of the heat exchanger. Hence the boundary condition to the hot side of the heat exchanger will be a function that is dependent on the solution to the catalyst model. To model the catalyst an energy balance is done for the fluid and catalyst walls respectively, resulting in the following equations [20],

$$\begin{aligned} \varepsilon \rho c_p \frac{\partial \theta_{cat}}{\partial \tau} &= -v \rho c_p \frac{\partial \theta_{cat}}{\partial x} + h_{cat} \gamma (\theta_{cat_w} - \theta_{cat}) \\ (1 - \varepsilon) \rho_{cat} c_{p_{cat}} \frac{\partial \theta_{cat_w}}{\partial \tau} &= h_{cat} \gamma (\theta_{cat} - \theta_{cat_w}) + k_m \gamma \Delta H C_m \end{aligned} \quad (36)$$

where  $\varepsilon$  is the porosity of the catalyst,  $\gamma$  is the surface to volume ratio of the catalyst channels,  $h_{cat}$  is the convective heat transfer coefficient and  $k_m$  is the mass transfer coefficient. For laminar flow in catalysts a value of the Sherwood number equal to 4 can be used. Giving that  $k_m = \frac{D Sh}{d_{cat}}$ , Where  $d_{cat}$  is the size of the catalyst channels and  $D$  is the diffusivity which can be obtained from  $D \propto T^{3/2}$ . It should be noted that the diffusivity will be evaluated at the mean temperature and that it will not change through the transient simulations. To obtain the convective heat transfer coefficient the approximation that  $Nu = Sh$  is used, such that  $h_{cat} = \frac{Shk}{d_{cat}}$  [21].

In order to get the expression for the concentration of methane,  $C_m$ , a mass balance is needed [20]. However for simplicity it is assumed that the concentration of methane in the catalyst wall always is zero, giving that the reaction rate only is determined by the rate of mass transport of methane to the wall,

$$-\varepsilon v \frac{\partial C_m}{\partial x} = k_m \gamma C_m \quad (37)$$

which has the solution,

$$C_m = d e^{-\frac{k_m \gamma x}{\varepsilon v}}. \quad (38)$$

The constant  $d$  is obtained from the boundary condition  $C_m(t, 0) = C_{m_{in}}(t)$ , where  $C_{m_{in}}(t)$  will be expressed as  $C_{m_{in}}(t) = C_0 + aH(t - t_0) + \dots$ , i.e a base concentration plus any number of step changes. This results in,

$$C_m(t, x) = C_{m_{in}}(t) e^{-\frac{k_m \gamma x}{\varepsilon v}}. \quad (39)$$

Equation, 36, is made dimensionless by parameters from the heat exchanger such that it will be possible to later solve for both of them together. However  $x$  is divided by the length of the catalyst such that  $X$  in both cases will go from 0 to 1.

$$\begin{aligned} X_{cat} &= \frac{x}{L_{cat}} & T_{cat} &= \frac{\theta_{cat} - \theta_{1,in}}{\theta_{1,in}} & t &= \frac{\tau}{\tau_r} \\ \alpha &= \frac{(1 - \varepsilon) \rho_{cat} c_{p_{cat}}}{\tau_r h_{cat} \gamma} & \delta &= \frac{k_m \Delta H}{h_{cat} \theta_{1,in}} \\ \delta &= \frac{k_m \Delta H}{h_{cat} \theta_{1,in}} & \zeta &= -\frac{\varepsilon L_{cat}}{v \gamma \tau_r} \\ \eta &= -\frac{h_{cat} L_{cat}}{v \rho c_p} & \psi &= \frac{k_m \gamma L_{cat}}{v \varepsilon} \end{aligned} \quad (40)$$

Which gives,

$$\begin{aligned}\zeta \frac{\partial T_{cat}}{\partial t} &= -\frac{\partial T_{cat}}{\partial X} + \eta(T_{cat_w} - T_{cat}) \\ \alpha \frac{\partial T_{cat_w}}{\partial t} &= (T_{cat} - T_{cat_w}) + \delta C_{m_{in}}(t)e^{\psi X_{cat}}.\end{aligned}\quad (41)$$

By using the Laplace transform with respect to the time variable,  $T_{cat}(t, X_{cat}) \rightarrow \hat{T}_{cat}(s, X_{cat})$  on Eq. 41 gives,

$$\begin{aligned}\zeta(s\hat{T}_{cat} - T_{cat}(0, X)) &= -\frac{\partial \hat{T}_{cat}}{\partial X} + \eta(\hat{T}_{cat_w} - \hat{T}_{cat}) \\ \alpha(s\hat{T}_{cat_w} - T_{cat_w}(0, X)) &= (\hat{T}_{cat} - \hat{T}_{cat_w}) + \delta C_{m_{in}}(s)e^{\psi X_{cat}}.\end{aligned}\quad (42)$$

The initial temperature for the gas and wall is set to zero, i.e equal to the inlet temperature. Substituting the Laplace transform of the wall temperature into the equation for the temperature of the gas gives,

$$\frac{\partial \hat{T}_{cat}}{\partial X} = \hat{T}_{cat}(-\zeta s - \eta + \frac{\eta}{\alpha s + 1}) + \frac{\delta C_{m_{in}}(s)}{\alpha s + 1}e^{\psi X_{cat}}.\quad (43)$$

The solution to Eq. 43 consists of the homogeneous and the particular solution. The homogeneous solution can directly be seen as,

$$\hat{T}_{cat_h} = m e^{(-\zeta s - \eta + \frac{\eta}{\alpha s + 1})X_{cat}}.\quad (44)$$

Where m is a constant, that needs to be determined from the boundary condition. The particular solution can be calculated from,

$$\hat{T}_{cat_p} = \hat{T}_{cat_h} \int \frac{\delta C_{m_{in}}(s)}{\alpha s + 1} e^{\psi X_{cat}} \hat{T}_{cat_h} dX_{cat} = \frac{\frac{\delta C_{m_{in}}(s)}{\alpha s + 1}}{\zeta s + \eta - \frac{\eta}{\alpha s + 1} - \psi} e^{\psi X_{cat}}.\quad (45)$$

The coefficient  $m$  is determined from the boundary condition  $\hat{T}_{cat}(s, 0) = \sum_{j=1}^N d_j u_{5j} e^{\beta_j}$ , i.e the solution from the heat exchanger at the fifth channel. It should be the average temperature of the cold channels, but as the number of channels increases the effect of the end channels will decrease and all the middle channels will have almost the same temperature. Hence for simplicity the fifth channel is chosen as the temperature out from the heat exchanger. Hence the coefficient will be  $m = \sum_{j=1}^N d_j u_{5j} e^{\beta_j} - \hat{T}_{cat_p}(s, 0)$ , and the solution to the catalyst will be given by,

$$\left( \sum_{j=1}^N d_j u_{5j} e^{\beta_j} - \hat{T}_{cat_p}(s, 0) \right) \hat{T}_{cat_h} + \hat{T}_{cat_p}.\quad (46)$$

Where  $\hat{T}_{cat_h}$  refers to the part  $e^{(-\zeta s - \eta + \frac{\eta}{\alpha s + 1})X}$ .

### 3.2.4 Solving for Both the Heat Exchanger and the Catalyst

To solve for the heat exchanger equations 11 to 15 needs to be scaled by  $T = \frac{\theta - \theta_{1, in}}{\theta_{1, in}}$  (instead of  $T = \frac{\theta - \theta_{1, in}}{\theta_{2, in} - \theta_{1, in}}$ ). This means that the boundary condition for at  $X = 0$  for the cold channels remains the same, see Eq. 22. But at  $x = 1$  the boundary condition for the hot channels will be the solution of the catalyst equations, i.e.  $\hat{T}_i(s, 1) = (\sum_{j=1}^N d_j u_{5j} e^{\beta_j} - \hat{T}_{cat_p}(s, 0)) \hat{T}_{cat_h}(s, 1) +$

$\hat{T}_{cat_p}(s,1)$   $i = 2,4\dots N$ , where  $\hat{T}_i(s,1) = \sum_{j=1}^N d_j u_{ij} e^{\beta_j}$   $i = 2,4\dots N$ . This means that the coefficients  $d$  can be solved from the equation system,

$$\begin{pmatrix} u_{11} & \dots & u_{1N} \\ (u_{21}e^{\beta_1} - \hat{T}_{cat_h}(s,1)u_{51}e^{\beta_1}) & \dots & (u_{2N}e^{\beta_N} - \hat{T}_{cat_h}(s,1)u_{5N}e^{\beta_N}) \\ u_{31} & \dots & u_{3N} \\ \dots & \dots & \dots \\ (u_{N1}e^{\beta_1} - \hat{T}_{cat_h}(s,1)u_{51}e^{\beta_1}) & \dots & (u_{NN}e^{\beta_N} - \hat{T}_{cat_h}(s,1)u_{5N}e^{\beta_N}) \end{pmatrix} \times \begin{pmatrix} d_1 \\ d_2 \\ d_3 \\ \dots \\ d_N \end{pmatrix} = \begin{pmatrix} 0 + \frac{ae^{-t_0s}}{s} + \dots \\ -\hat{T}_{cat_p}(s,0)\hat{T}_{cat_h}(s,1) + \hat{T}_{cat_p}(s,1) \\ 0 + \frac{ae^{-t_0s}}{s} + \dots \\ \dots \\ -\hat{T}_{cat_p}(s,0)\hat{T}_{cat_h}(s,1) + \hat{T}_{cat_p}(s,1) \end{pmatrix}. \quad (47)$$

$B$   $K$

The coefficients are obtained by  $d = B^{-1}K$ . The temperature in the heat exchanger can be obtained from,

$$\hat{T}_i = \sum_{j=1}^N d_j u_{ij} e^{\beta_j X} \quad i = 1,2,\dots,N \quad (48)$$

### 3.2.5 Response in Time Domain

The temperature in the frequency domain is obtained by Eq. 48, however in order to get the temperature as a function of time the equation must be inverted by Laplace inversion. Up to this point it is worth noting that the solution is analytical, but since the expression is too complex to carry out the Laplace inversion analytically a numerical method has to be used.

The definition of the inversion formula is,

$$T(t,X) = \frac{1}{2\pi i} \int_{a-i\infty}^{a+i\infty} e^{st} \hat{T}(s,X) ds \quad (49)$$

Where  $a > 0$  is arbitrary but must be chosen so that it is greater than the real parts of all singularities of  $\hat{T}(s,X)$ . Since  $T(t,X)$  is real function Eq. 49 can be written as,

$$T(t,X) = \frac{2e^{at}}{\pi} \int_0^\infty Re[\hat{T}(s,X)] \cos(wt) dw \quad (50)$$

where  $s = a+iw$ . For this case there will be no singularities right of the origin, and  $a$  can therefore be chosen appropriately such that the error can be controlled. If the integral is discretized using the trapezoidal rule with a step size  $\tilde{h}$ , Eq. 50 can be written as,

$$T(t,X) \approx T(t,X)_{\tilde{h}} = \frac{\tilde{h}e^{at}}{\pi} Re[\hat{T}(a,X)] + \frac{2\tilde{h}e^{at}}{\pi} \sum_{k=1}^\infty Re[\hat{T}(a + ik\tilde{h},X)] \cos(k\tilde{h}t). \quad (51)$$

By letting  $\tilde{h} = \frac{\pi}{t}$  and  $a = \frac{G}{2t}$  the equation can be written as,

$$T(t,X) = \sum_{k=0}^\infty (-1)^k c_k(t,X) \quad (52)$$

where

$$\begin{aligned} c_0(t) &= \frac{e^{G/2}}{2t} \left( \hat{T}\left(\frac{G}{2t}, X\right) - 2\text{Re}[\hat{T}\left(\frac{G}{2t} + \frac{i\pi}{t}, X\right)] \right) \\ c_k(t) &= -\frac{e^{G/2}}{t} \left( \hat{T}\left(\frac{G}{2t} + \frac{i\pi}{t} + \frac{ik\pi}{t}, X\right) \right). \end{aligned} \quad (53)$$

By calculating the coefficients for the wanted times,  $t$ , and an appropriate  $A$ , the temperature  $T$  can be obtained as a function of time[22]. It is worth mentioning that the result is the dimensionless temperature as a function of the dimensionless time. In order to view the result in terms of physical quantities the result is scaled with Eq. 16 and Eq. 40.

### 3.2.6 Implementation

In order to obtain the solution the program Matlab is used. The eigenvalues and the eigenvectors of the matrix  $\bar{A}$  are, for each time step, obtained using the Matlab commando  *eig* . The coefficients are determined from the boundary conditions and are calculated from Eq. 47. Which gives that the solution in the Laplace plane is given by Eq. 48. To obtain the solution as a function of time the coefficients,  $c_k(t)$  are calculated from Eq. 53, which finally means that the temperature in the heat exchanger can be calculated from Eq. 52.

### 3.2.7 Error Analysis

The solution method contains no approximations until the inverse of the Laplace transform has to be obtained. The numeric inversion of the Laplace transform has three sources of errors. The discretization error associated with approximating  $T(t, X)$  with  $T(t, X)_{\tilde{h}}$ , the truncation error associated with calculating the infinite series and the roundoff error associated with the addition and multiplication that occurs when calculating  $T(t, X)_{\tilde{h}}$ . Normally the discretization error for the trapezoidal rule is bounded by  $\mathcal{O}(\tilde{h}^2)$ . However in this case the special trigonometric structure of  $T(t, X)_{\tilde{h}}$  gives that it can be seen as a Fourier series. By using an alternative way of getting  $T(t, X)_{\tilde{h}}$  the error can in the end be estimated by,

$$|e(t)| \leq \frac{C e^{-G}}{1 - e^{-G}}, \quad (54)$$

if  $T(t, X)_{\tilde{h}}$  can be limited by a constant  $C$  [22]. The infinite series has to be truncated, this is simple done by choosing a number to sum up to. Then the error associated with this is roughly of the size of the last term in the series. It seems like the error can be made arbitrary small by choosing  $G$  arbitrary large, however even if the discretization error is small the total error will still be bound by the largest error term, i.e the sum has to include more terms in order for the total error to decrease. Another problem with choosing  $G$  arbitrary large is that the prefactor  $\frac{e^{G/2}}{2t}$  can become very large, causing roundoff errors. There is hence a trade off between the discretization error and the roundoff error, which is dependent on the machine precision [22].

## 3.3 CFD Simulation of a Heat Exchanger

Computational fluid dynamics (CFD) simulates flow behavior with the use of appropriate computational models. One of the major benefits using CFD software is that the cost for performing different fluid simulations on a computer model are much lower compared to assembling, modifying and performing experiments on the actual geometry. Computational fluid dynamic softwares

are therefore an useful tool when performing heat exchanger analyses. This section presents an overview of the general theory used to perform the CFD-simulations included in this thesis, including information about the models, numerical schemes and boundary conditions.

### 3.3.1 Governing Equations

In order to perform a simulation over a heat exchanger with the use of CFD-software, a set of equations needs to be solved. The equations are the continuity, momentum and energy equations. The mentioned equations are referred to as the governing equations and are presented in this section.

The continuity equation is a material balance over a fluid element. It is for an incompressible fluid written as,

$$\frac{\partial U_j}{\partial x_j} = 0 \quad (55)$$

where U is the velocity, x the direction and the index j refers to the number of dimensions included.

The momentum equation represents a momentum balance over a volume. The momentum equation can be written in tensor notations as,

$$\frac{\partial U_i}{\partial t} + U_j \frac{\partial U_i}{\partial x_j} = -\frac{1}{\rho} \frac{\partial P}{\partial x_i} + \frac{1}{\rho} \frac{\partial \tau_{ij}}{\partial x_j} + g_i. \quad (56)$$

Where U is the velocity and x is the direction. The pressure is written as P and the density as  $\rho$ ,  $\tau$  represents the viscous stresses and g the gravity. The index letter j represent the different dimensions, summarized over all dimensions in the equation. The index letter i is constant for each equation and instead increases the number of equations to the number of dimensions present.

The stress term can for Newtonian fluids be rewritten as  $\tau_{ij} = \mu \left( \frac{\partial U_i}{\partial x_j} + \frac{\partial U_j}{\partial x_i} \right)$ , giving that equation 56 can be written as,

$$\frac{\partial U_i}{\partial t} + U_j \frac{\partial U_i}{\partial x_j} = -\frac{1}{\rho} \frac{\partial P}{\partial x_i} + \nu \frac{\partial}{\partial x_j} \left( \frac{\partial U_i}{\partial x_j} + \frac{\partial U_j}{\partial x_i} \right) + g_i. \quad (57)$$

Where  $\nu$  which represents the kinematic viscosity.

Energy is included in several different forms in a fluid flow. The total energy in a flow can therefore be seen as the sum of its kinetic, thermal, chemical and potential energy. The equation for the total energy can be seen as,

$$\frac{\partial h}{\partial t} = -\frac{\partial}{\partial x_j} \left[ hU_j - k_{eff} \frac{\partial T}{\partial x_i} + \sum_n m_n h_n j_n - \tau_{kj} U_k \right] + S_h. \quad (58)$$

Where h referees to the total energy,  $m_n$  the mass fraction and  $j_n$  the diffusional flux for the species.

### 3.3.2 Turbulence Modeling

As soon as the flow turns turbulent it becomes very hard to fully solve the Navier-Stokes equations, due to turbulent length and time scales. In order to solve a turbulent flow, approximations

have to be made. One common approximation for turbulent flows is the Reynold decomposition. It divides properties in mean and fluctuating terms, as shown for the velocity in the equation below.

$$U_i(x,t) = \overline{U}_i(x,t) + u_i(x,t) \quad (59)$$

where  $\overline{U}_i(x,t)$  is the mean velocity and  $u_i$  is the fluctuating term. A consequence of the Reynold decomposition is that the flows are now treated statistically. One important property of turbulence is that the time scales differs significantly within the flow, of which small turbulent eddies have smaller time scales than for those of larger fluid movements. By choosing appropriate time period while time averaging, the turbulence fluctuations and the larger fluid movements becomes separated. Implementing these steps upon the Navier-Stokes equations results in the Reynold averaged Navier-Stokes equations (RANS). The RANS equation is, after some re-arranging, presented below,

$$\frac{\partial \langle U_i \rangle}{\partial t} + \langle U_j \rangle \frac{\partial \langle U_i \rangle}{\partial x_j} = -\frac{1}{\rho} \frac{\partial}{\partial x_j} \left[ \langle P \rangle \delta_{ij} + \mu \left( \frac{\partial \langle U_i \rangle}{\partial x_j} + \frac{\partial \langle U_j \rangle}{\partial x_i} \right) - \rho \langle u_i u_j \rangle \right] \quad (60)$$

where  $\delta_{ij}$  is the Kronecker delta and the term  $-\rho \langle u_i u_j \rangle$  is refereed to as the Reynold stress.

However, the new Reynold stress tensor is unknown and therefore needs to be modeled. One approximation to write the Reynold stress tensor is in terms of the mean velocity gradients. This is called the Boussinesq approximation. Due to the approximation, solutions obtained this way will also be approximations of the real solution. The Boussinesq approximation models the momentum transport of a diffusive process. If this is implemented upon the RANS equations, the following equation is obtained,

$$\frac{\partial \langle U_i \rangle}{\partial t} + \langle U_j \rangle \frac{\partial \langle U_i \rangle}{\partial x_j} = -\frac{1}{\rho} \frac{\partial \langle P \rangle}{\partial x_i} - \frac{2}{3} \frac{\partial k}{\partial x_i} + \frac{\partial}{\partial x_j} \left[ (\nu + \nu_T) \left( \frac{\partial \langle U_i \rangle}{\partial x_j} + \frac{\partial \langle U_j \rangle}{\partial x_i} \right) \right] \quad (61)$$

where  $k$  is the turbulent kinetic energy per unit mass and  $\nu_T$  the turbulent viscosity. In order to solve the equation above,  $\nu_T$  needs to be modeled.  $\nu_T$  is dependent upon appropriate velocity and length scales ( $u, l$ ) which needs to be modeled. There are several models based upon the idea of turbulent viscosity, each depending on a certain number of additional transports equations to model the velocity and length scales. Generally speaking, the model which includes more equations often provides better results, at the cost of longer simulation time. Models which includes two equations is rather common were one equation solves for the length scale and one for the velocity. Most commonly known of the two equation models are  $k$ - $\epsilon$ -model and  $k$ - $\omega$ -model. Each model and each model variation have its own strengths and weaknesses. The model chosen in this thesis is the  $k$ - $\omega$ -SST model.

### 3.3.3 The $k$ - $\omega$ SST model

The  $k$ - $\omega$  model is a popular two-equation turbulence model. In order to model the Reynold stresses, the  $k$  and  $\omega$  (the specific dissipation) is modeled. The  $k$ -equation is modeled as

$$\frac{\partial k}{\partial t} + \langle U_j \rangle \frac{\partial k}{\partial x_j} = \nu_T \left[ \left( \frac{\partial \langle U_i \rangle}{\partial x_j} + \frac{\partial \langle U_j \rangle}{\partial x_i} \right) \frac{\partial \langle U_i \rangle}{\partial x_j} \right] - \beta k \omega + \frac{\partial}{\partial x_j} \left[ \left( \nu + \frac{\nu_T}{\sigma_k} \right) \frac{\partial k}{\partial x_j} \right] \quad (62)$$

and the  $\omega$  equation is modeled as

$$\frac{\partial \omega}{\partial t} + \langle U_j \rangle \frac{\partial \omega}{\partial x_j} = \alpha \frac{\omega}{k} \nu_T \left[ \left( \frac{\partial \langle U_i \rangle}{\partial x_j} + \frac{\partial \langle U_j \rangle}{\partial x_i} \right) \frac{\partial \langle U_i \rangle}{\partial x_j} \right] - \beta^* \omega^2 + \frac{\partial}{\partial x_j} \left[ \left( \nu + \frac{\nu_T}{\sigma_\omega} \right) \frac{\partial \omega}{\partial x_j} \right] \quad (63)$$

The turbulent viscosity is then calculated as

$$\nu_T = \frac{k}{\omega} \quad (64)$$

The  $k-\omega$  shear stress transport (SST) model uses the  $k-\omega$  model in the near wall regions. In free stream, the model switches into a  $k-\epsilon$  behavior and is thereby reducing the sensitivity regarding inlet free stream turbulent properties. The  $k-\omega$  SST model is good at handling separating flow and adverse pressure gradient but does over produce turbulence in areas with large normal strain, such as stagnation regions.

### 3.3.4 Simulations Methodology

The  $k-\omega$  SST model was used for all the simulations in this thesis work, which were all conducted with the use of Ansys FLUENT, version 15.0. The model were chosen because of its strength in modeling the regions close to the wall, where the heat transfer occurs. In addition, a previous study have shown successful results with simulations over a plate heat exchanger while using the  $k-\omega$  SST model [23]. In order to reach good simulation results, the sizing and shape of the computational cells are of importance, specially in areas with large gradients of the important variables. Regions with large changes therefore requires a more dense mesh with smaller computational cells. In order for the  $k-\omega$  SST model to be accurate, a value  $y^+$  of maximum 1 is required for all cells adjacent to the walls, where  $y^+$  is defined as

$$y^+ = \frac{yu_*}{\nu}, \quad (65)$$

where  $y$  is the distance to the wall,  $\nu$  is the viscosity of the fluid and  $u_*$  is the characteristic velocity scales at the wall.  $y^+$  values are used to estimate the impact of the Reynold stress tensor.

In order to meet the requirement of an  $y^+$  value of maximum 1, inflation layers were used in the areas close to the walls. A total of 5 inflation layers were used, with a first layer thickness of  $1 \times 10^{-5}$ m. The growth rate for the inflations layers were set to 1,2. The inlet and outlet surfaces which were to have periodic boundary conditions were given match control, thereby creating a identical mesh on both surfaces. The automatic meshing method in Ansys was used for creating all of the meshes in this thesis, which were constructed mainly in the shape of tetrahedrons.

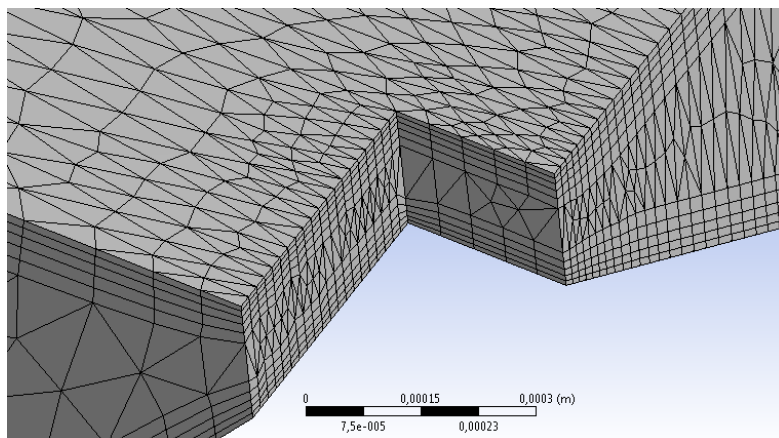


Figure 14: The inflation layers on the surfaces in contact with the plates.

The fluid simulated was pure air since the small amounts of other substances such as methane and CO were considered too small to have any affect on the flow profile. Constants values for density, heat capacity, thermal conductivity and fluid viscosity were chosen. These were chosen for air at a temperature of 300 C°. The properties of water was in this case taken for 25 C°. The values for both of the cases are presented in the Table 4.

Table 4: Material data

Compound	Density ( $\frac{kg}{m^3}$ )	Specific Heat ( $\frac{j}{kgK}$ )	Thermal Conductivity ( $\frac{w}{mK}$ )	Viscosity ( $\frac{kg}{ms}$ )
Air	0.6159	1047	0.0454	$3.2766 \times 10^{-5}$
Water	995.7	4179	0.6	0.000798

The numerical scheme used during all of the simulations was the upwind discretization scheme. Simulations started with first order upwind scheme and were later changed to second order upwind scheme when the simulations were considered stable enough.

The under relaxation factors were adjusted for each simulation in order for them to converge properly. Other settings apart from those mentioned above were set with default values in Ansys Fluent. All simulations were made in steady state mode.

### 3.3.5 Boundary Conditions for the Simulations

Stationary no slip walls were chosen as a boundary conditions for the upper and lower plates in the heat exchanger segment, both with a roughness constant of 0.5. The material chosen was steal, for which the default properties within Fluent were used. Both walls were given a constant temperature of 623K, heating the cold stream of gas. This is however a simplification of reality, since the temperature in the hot plates are lower towards the end of the plate. In theory however, the temperature difference of a counter current plate heat exchanger is approximately the same throughout the heat exchanger. With fixed values on the walls for the simulated segment, this will then not be completely true since the temperature difference will decrease to some extent through the length of the segment, but it was still considered to be sufficiently realistic assumption.

The inlet and outlet were set to a periodic boundary condition. This means that the outlet flow profile of the segment then continuously enters as a inlet. With the periodic boundary condition, the flow profile for the small symmetric heat exchanger segment will take the shape of an infinite long heat exchanger with the same width as the simulated segment. This periodic boundary conditions were chosen in order to save computational time. The periodic inlet temperature was set to 553 K, creating a temperature difference of 70 K towards the walls. The mass flow was set to 0.2 kg/s for the whole heat exchanger, which was considered a representable duty for the heat exchanger in reality. The mass flow for each study is dependent on the number of channels in the heat exchanger and the width of the simulated segment. The mass flow for the different simulation cases can be seen in Table 5. A relaxation factor of 0.5 was chosen for the periodic boundary condition and the number of iterations for the periodic conditions were set to four.

The two sides of the segment were given a stationary slip wall boundary condition with zero heat flux. The roughness constant were chosen to zero, essentially forming an frictionless, adiabatic wall. This boundary condition was considered the most appropriate when only a small symmetry segment was simulated.

Table 5: Mass flows

Geometry setup	Compound	mass flow ( $\frac{kg}{s}$ )
Symmetric segment, 30°	air	0,00044
Symmetric segment, 80°	air	0,00423
Symmetric segment, 80°	water	0,11250
Whole width, 30°	air	0,00645

In the simulations where no gap between the plates were present, additional walls were created where the heat exchanger plates were considered to merge into each other. These walls were given the same physical conditions as the upper and lower plates, but were considered adiabatic. This was considered acceptable since the flow in the region close to these walls was small, and therefore had limited effect on the system as whole.

### 3.3.6 Simulated Geometries

The different geometries used in this thesis are presented in this section together with a description of the simplifications that were made.

An adjustment made for all the different geometries in this thesis was the modified shape of the corrugations. Triangular corrugations was used instead of sinus shaped corrugations in order to simplify the mesh. Another simplification made in the simulations was that only one channel was simulated. The inlet stream was in all cases chosen to be the cold stream in the heat exchanger. This was done in order to save computational time.

The period of the corrugations were chosen to 10 mm, and its amplitude 2.5 mm on each plate. The maximum distance between the plates is therefore 5 mm. The width and length of the different symmetry segments were different, each depending on its Chevron angle. A sharper Chevron angle resulted in smaller but longer segments, while segments with lower angles were wider and shorter. For exact sizes on the different constellations, see Table 6.

Table 6: Different geometries

Geometry	Length (mm)	Width (mm)
Symmetric segment, 30°	20,000	11,547
Symmetric segment 80°	57,588	10,154
Whole width 30°	20,000	161,658

The different geometries used for the simulations are presented in Figures 15 to 17.

Figure 15 illustrates the symmetric geometrical segment used during the simulations. As shown in the picture, corrugations are slicing the geometry from left to right with an angle of 30°. Identical corrugations but this time in the direction from right to left are placed on the opposite side of the segment, thereby forming the geometry inside of a plate heat exchanger with Chevron corrugations. It should be noted that the fluid travels in the z-direction for all of the Figures 15, 16 and 17.

In Figure 16 the geometry of the full width of a Chevron corrugated heat exchanger is shown. It should be noted that the geometry in Figure 15 is identical to parts of the geometry in Figure 16.

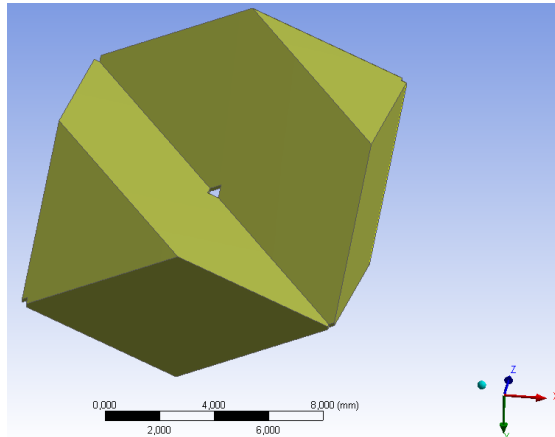


Figure 15: Symmetric heat exchanger segment with a Chevron angle of  $30^\circ$ .

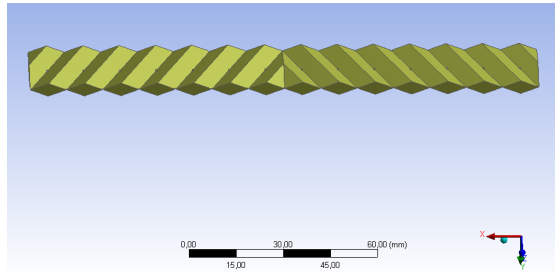


Figure 16: Whole width of the heat exchanger with a Chevron angle of  $30^\circ$ .

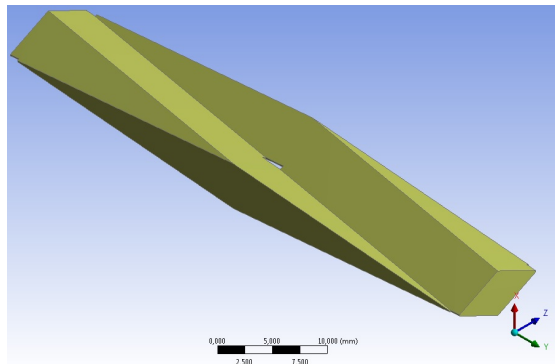


Figure 17: Symmetric heat exchanger segment with a Chevron angle of  $80^\circ$ .

Figure 17 displays the geometrical segment used for the simulations for the Chevron heat exchanger with an inclining angle of  $80^\circ$ . The inlet and outlet in this geometrical setup were therefore the longer sides of the geometry. The hole in the middle was created in order to better replicate the actual geometry where the plates were pressed into each other, as well to simplifying the mesh in these regions.

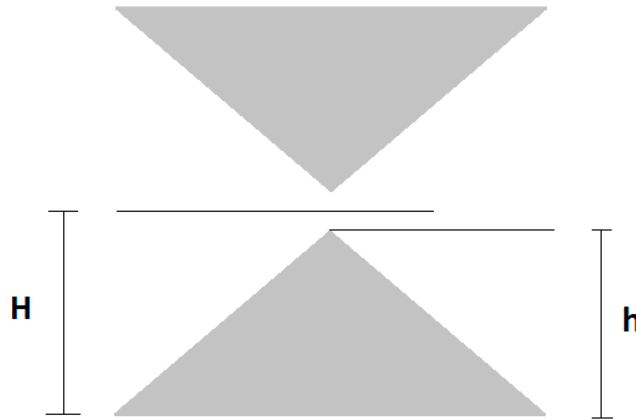


Figure 18: Heights used for the definition of gap distance.

Previous studies have shown that a small gap between the plates might be used in order to not get a very dense mesh where the plates were in contact with each other [23]. The gap distance is defined from the heights in Figure 18, and is defined as  $h/H$ , i.e. the quota between the height of the corrugations divided by height of the corrugations plus the added space between the plates. A quota value of 1 would therefore mean that the plates are in contact with each other. It is however important to know if this small gap have any impact on the flow field and heat transfer for the segment. A study regarding this was therefore done where four different gap sizes were tested and compared to a case where the plates were in contact with each other.

Most of the correlation data found regarding plate heat exchangers were derived for liquids. In order to verify that the same correlations still holds for gases, a simulation with water instead of air was performed in order to see if there was any deviation compared to the chosen correlation. A heat exchanger segment with contact between the plates and a Chevron angle of  $80^\circ$  was used, but this time the fluid was set to water with an inlet temperature of  $20^\circ C$ . The temperature of the walls were set to  $90^\circ C$ , thereby creating a temperature difference between fluid and walls of  $70^\circ C$ . The water data was gathered for water at a temperature of  $25^\circ C$ , which is close to the average temperature of the flow.

As mentioned earlier, the flow pattern is strongly dependent on the Chevron angle in the plate heat exchanger. Higher Chevron angels tend to force the flow to tumble forward in the direction normal to the inlet, while the flow profile for lower angles follows the channels and bounces between the outer walls of the heat exchanger. One objective is to successfully replicate these flow patterns with the use of CFD simulations. Since periodic inlet and outlet boundary conditions were used in this thesis in order not to simulate the full length of the heat exchanger, it was of importance to make sure that the chosen width of the symmetry segment did not affect the results. This is done by creating two different models with different width by comparing the results. Apart from the width, every setting were to be the same for the two models except for the mass flow which was adjusted so that the mass flux for both models were equivalent.

In order to gather information regarding how the flow profile within the heat exchanger looked

like in different geometrical setups, a flow analysis was performed for heat exchanger segment with Chevron angles of  $30^\circ$  and  $80^\circ$ . The aim for this study was to gather information about the thickness of the thermal boundary layer over different areas of the geometry, and to see in which zones turbulence was created inside of the heat exchanger segment.

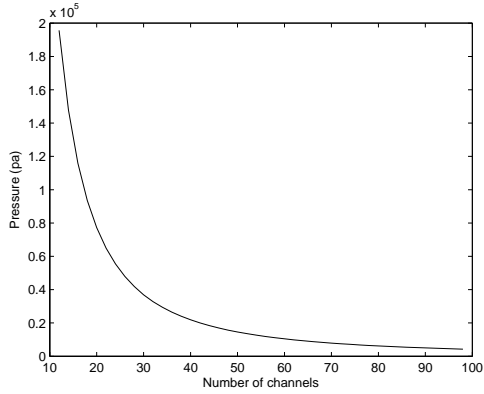
## 4 Results

### 4.1 System Simulations-Steady State Condition

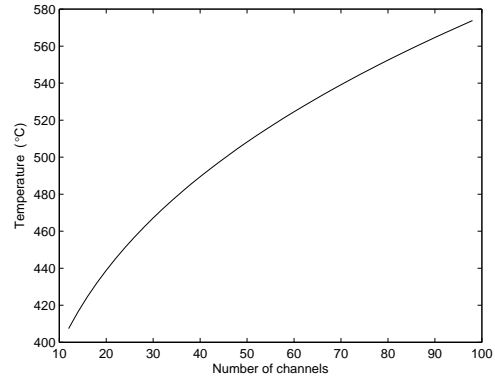
In order to get a basic understanding of the size needed for the heat exchanger the steady state model is applied. The heat exchanger is given the dimensions of  $L = 0.65m$  and  $B = 0.17m$ , which is a rough estimate of the space available in a truck. The plate design used, is plates with a chevron angle of  $30^\circ$  and a maximum height in the channels of  $5mm$ , but with the design allowing for two channels to take the space of  $5mm$ . With a plate thickness of  $0.5mm$ , 62 channels will take the space of  $0.192m$ , where channels are referring to the space between two plates in the heat exchanger. The catalyst used has a length of  $0.25m$  and a diameter of  $0.27m$ . The channels in the catalyst are square with a length of  $1mm$  and a wall thickness of  $0.15mm$

For typical operating conditions,  $\dot{m} = 0.2kg/s$ ,  $T_{c_{in}} = 280^\circ C$  and  $y = 1200ppm$  methane, the temperature, the pressure drop and the effectiveness are plotted as a function of the number of channels in the heat exchanger, which is shown in Figure 19. It can be noted that the calculations are only done for an even amount of channels with an equal amount of mass flow in the cold and hot side.

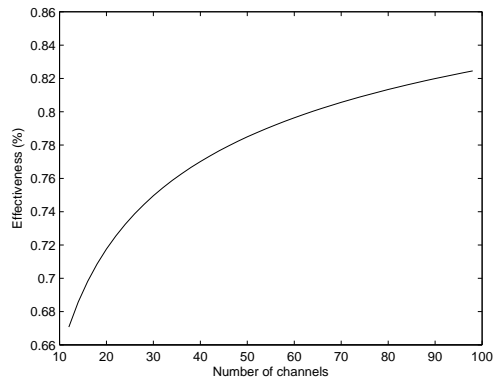
It can be seen that for these operating conditions the use of 62 channels will give a temperature out from the heat exchanger at  $527.6^\circ C$ , which should be more than sufficient to obtain a high conversion of methane in the catalyst. The pressure drop for 62 channels is seen to be  $9.85kPa$ . Since this number of channels gives a sufficiently low pressure drop and a high temperature into the catalyst, it will be used as a base design for the heat exchanger. In Figure 19c the effectiveness, defined by equation 8, is shown as a function of the number of channels. However even if these conditions are roughly averaged, the conditions are in reality changing all the time. To get an understanding of between what values the temperature, the pressure drop and the over heat transfer will vary, the steady state model is applied to some typical driving data, where the result is shown in Figure 20.



(a)



(b)



(c)

Figure 19: Average conditions (a) pressure drop (b) temperature into the catalyst (c) effectiveness.

Note that in Figure 20, transient data is given fixed boundary conditions to the steady state model, hence the result only show what would happen if each point of calculation is run until steady state. However the pressure drop and the overall heat transfer coefficient are changing instantaneously, hence Figures 20a and 20c give a correct picture of what will happen at each operating point. The temperature does however just show what will happen if each point of calculation would be run until steady state, and does therefore not capture the dynamics of the heat exchanger, it just gives a picture of what the upper and lower bounds will be. In order to see how the temperature will change with respect to transient data, the transient model has to be used.

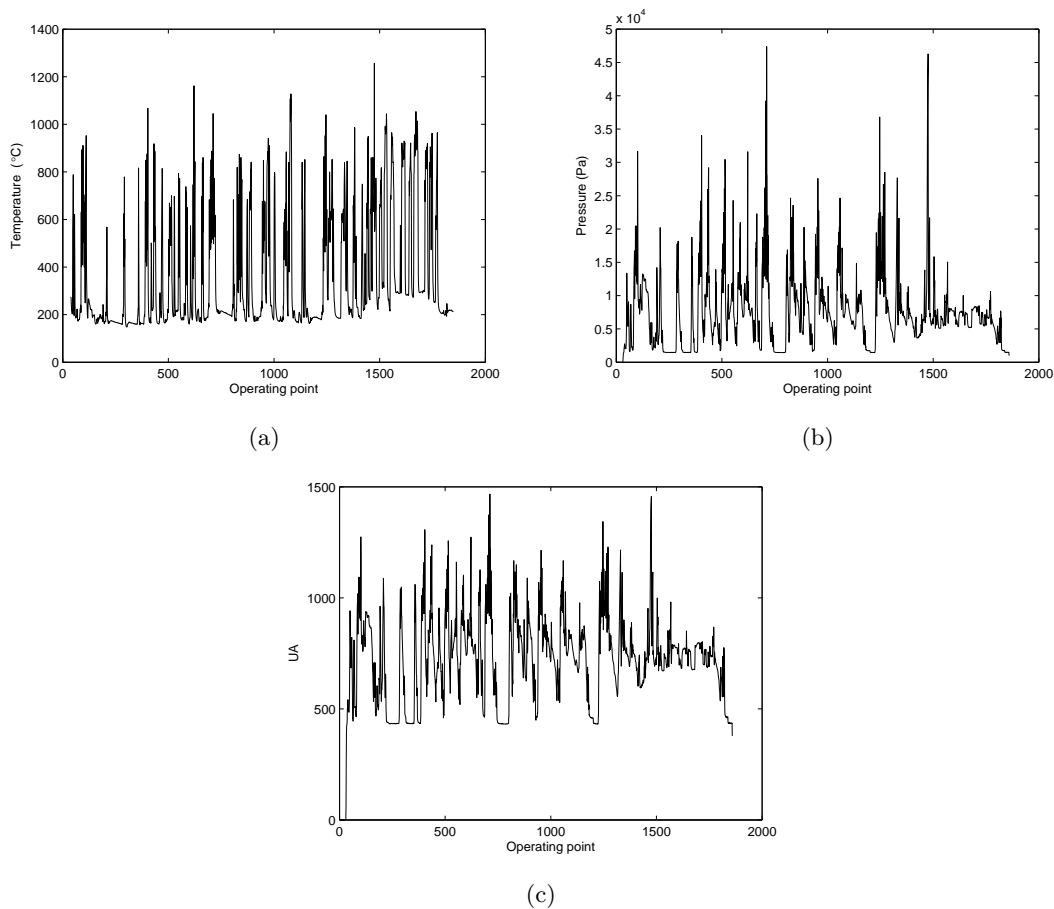


Figure 20: Results from the steady state model at different operating points (a) the temperature into the catalyst (b) pressure drop (c) overall heat transfer coefficient.

## 4.2 System Simulations - Transient Analysis

The first transient analysis was done with the same boundary conditions as in Figure 19 and is performed with 62 channels. In order to get an understanding of what time is needed before steady state is reached.

In Figure 21a the temperature out from the heat exchanger, i.e. into the catalyst is shown, and in Figure 21b the temperature out from the catalyst, i.e into the catalyst is shown. It can be noted that it takes somewhat more than 1000 seconds until steady state is reached, but that the temperature goes above  $400^{\circ}\text{C}$  in around 300 seconds. It can also be seen that the temperature out from the catalyst reaches a temperature that is around  $62^{\circ}\text{C}$  warmer than into the catalyst, which is the theoretical value if all methane will react.

To study the effect when the inlet conditions are changing, first only the methane is changed such that this parameter can be evaluated. The change of methane is shown in Figure 22a and the result of this change on the temperature into the catalyst can be seen in Figure 22b.

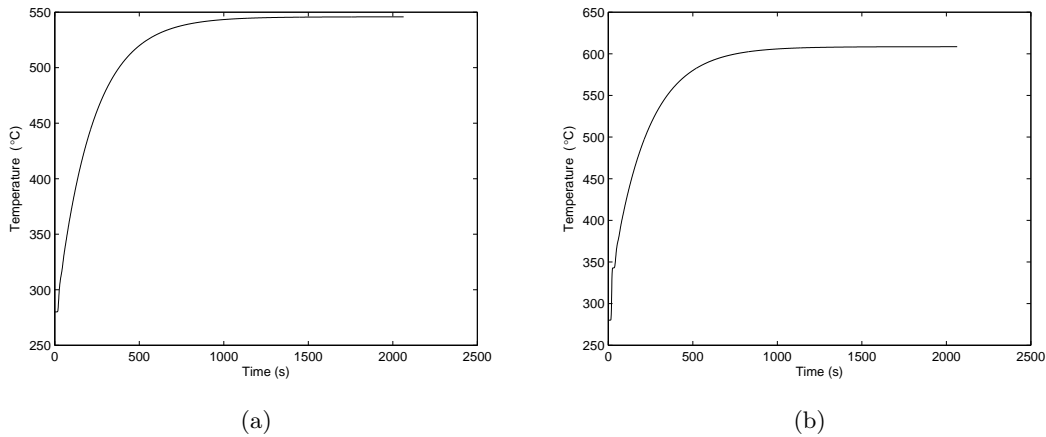


Figure 21: The transient model run with constant values (a) temperature into the catalyst (b) temperature out from the catalyst.

It can be seen that the changes in the temperature into the catalyst corresponds to the behavior of the methane, early there is a very low concentration of methane which leads to a temperature drop. But then there is more methane for a while, leading to an increase in the temperature, and near the end there is a higher average of methane leading to a temperature that is higher than for the constant values. To see how the model reacts to changing the in-temperature, the amount of methane is kept constant, but typical data for the in-temperature is applied. The in-temperature can be seen in Figure 23a and the response on temperature into the catalyst can be seen in Figure 23b.

It can be noted that the inlet temperature for a while drops down to around  $150^{\circ}\text{C}$ , then it has a rapid changing behavior and towards the end it reaches a larger mean average temperature. The response of this is that the temperature at first drops but towards the end reaches a higher temperature. It can also be seen that the response of the temperature into the catalyst from changing the inlet temperature gives a much smoother behavior compared to when the concentration of methane was changing. However the very rapid changing behavior is due to that the temperature is changing fast in the catalyst and that the solution is calculated at the end of the heat exchanger. If the temperature is plotted in the middle of the heat exchanger, shown in Figure 22c, the thermal mass of the heat exchanger will dampen the fluctuations.

The effect when both the temperature and the methane is changing is shown in Figure 24a. It is also desirable to include the effect of changing mass flow. However when deriving the governing equations the mass flow is not time dependent, it is a constant. There is hence no function that can be transformed into the Laplace plane where the solution is being calculated. It is still possible to set the mass flow to a new value for each time step, but since this is done without actually having a continuous function in the Laplace plane, it leads to very direct changes of the solution. But since the mass flow does have an impact on the result it is still important to include it. When the mass flow is changing it is however likely that the solution will change quickly, i.e changing the mass flow should still give a correct solution despite being a constant in the equations. What is done is that the mass flow is averaged over shorter time spans and each section is run with the different averaged mass flows, the result is shown in Figure 24b.

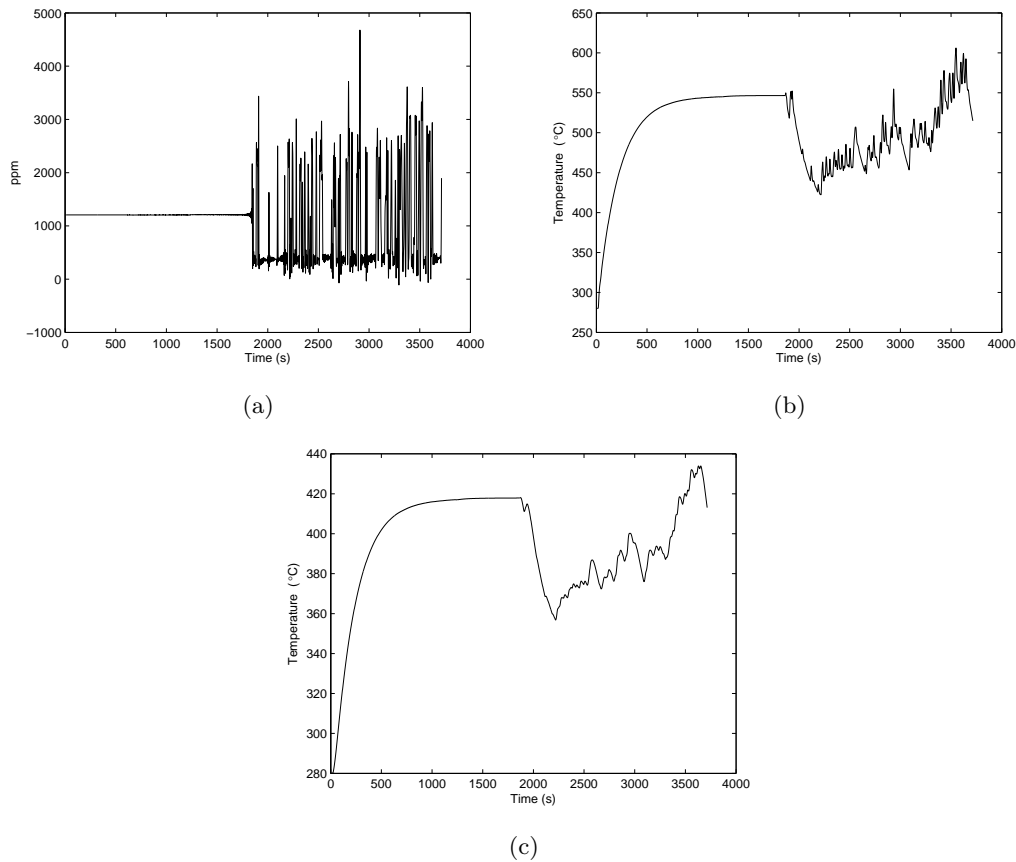
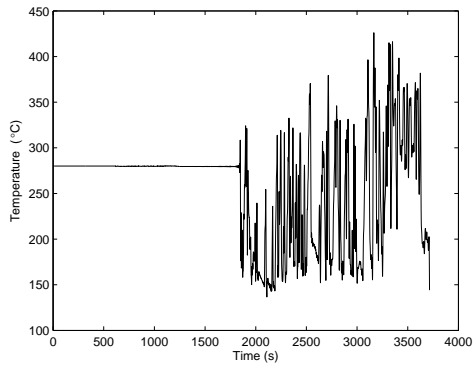


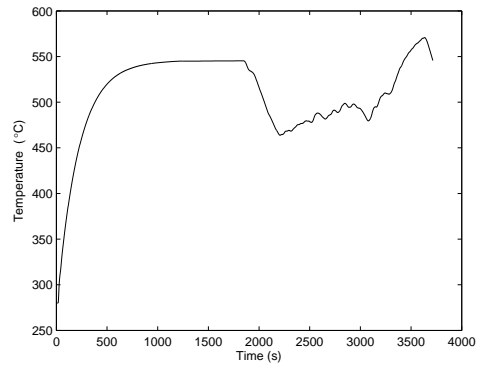
Figure 22: The transient model run with changing concentration of methane (a) ppm methane (b) temperature into the catalyst (c) temperature in a cold channel in the middle of the heat exchanger.

It can be seen from Figure 24a that when both the methane and the inlet temperature are changing, the low values of both of these at the start leads to a temperature decrease into the catalyst. However when the mass flow also is changed, Figure 24b, the temperature drops much slower since in the section where the methane and inlet temperature are low, the average mass flow is also low. The lower mass flow leads to a longer resident time in the heat exchanger which explains the higher temperature.

But still the temperature goes below  $400^{\circ}C$ , to evaluate if it is possible to keep the temperature sufficiently high, despite the large drop of both methane and in-temperature, the  $h$ -value is increased by 50%. This is achieved by increasing the chevron angle of the plates, looking at Figure 12 it can be seen that an increase of 50% roughly corresponds to changing the chevron angle from  $30^{\circ}$  to  $50^{\circ}$ . The result of the increased  $h$ -value when all the in-data parameters are changing can be viewed in figure 25a. Another option to keep the temperature sufficiently high into the catalyst is to increase the size of the heat exchanger. This is done by increasing the number of channels from 62 to 92, the result is shown in Figure 25b.

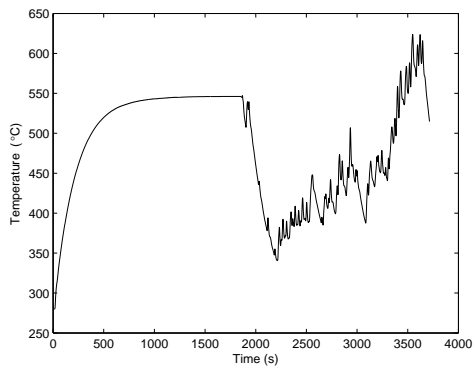


(a)

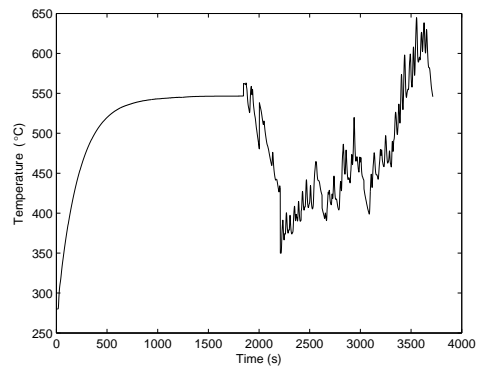


(b)

Figure 23: The transient model run with changing in-temperature (a) temperature into the heat exchanger (b) temperature into the catalyst.



(a)



(b)

Figure 24: Temperature into the catalyst (a) changing methane and in-temperature (b) all in-parameters changing.

It can be seen that the temperature for both cases stays higher, but that increasing the  $h$ -value is more effective. However towards the end for the increased  $h$ -value the temperature reaches values above  $700^{\circ}\text{C}$ .

The model is further used to evaluate what happens when the changing inlet temperature, methane and mass flow is directly applied, i.e without first using constant values such that the heat exchanger and catalyst already are warm when the data is applied. Since the catalyst model does not include that the reaction of methane is dependent on the temperature in the catalyst, all of the methane will react independent of the temperature. This means that when the data is directly applied, the initial temperature will in reality be too low to achieve full conversion of methane. Hence the simulations will not give a correct picture of what will happen, but will be an overestimation of what will happen. It can still be interesting to see if the temperature into the catalyst will go above  $400^{\circ}\text{C}$  even when all of the methane is reacting, and to see how long

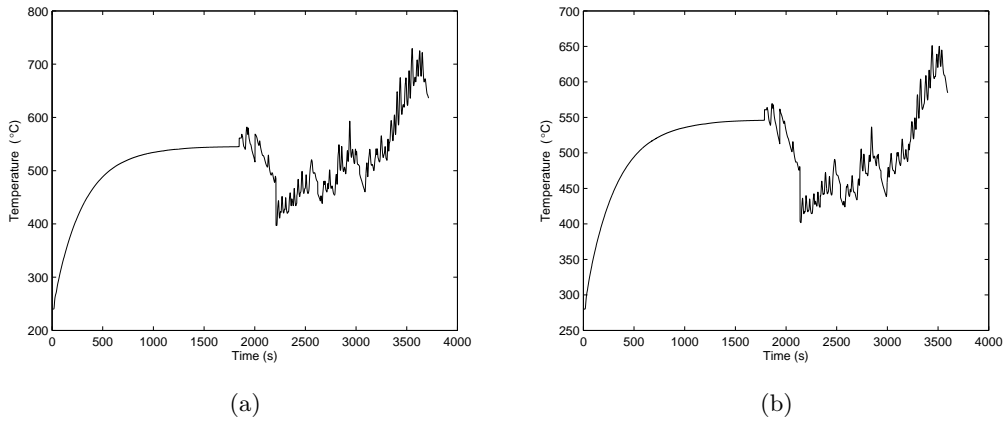


Figure 25: Temperature into the catalyst (a) increased  $h$ -value (b) 92 channels.

time it will take. In Figure 26a both changing methane and inlet temperature is applied from start of the simulation and in Figure 26b the mass flow is changing as well.

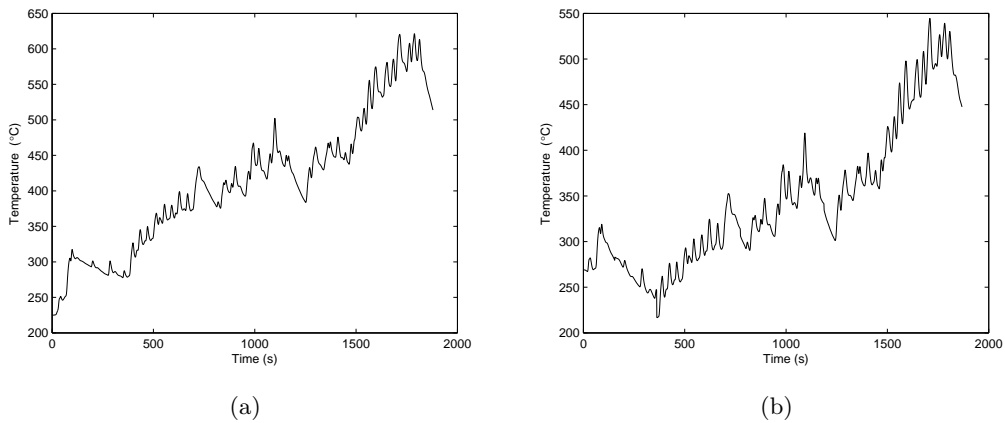


Figure 26: Data applied from start (a) changing methane and inlet temperature (b) all inlet parameters changing.

It can be concluded that even when all the methane is reacting it takes around 1500 seconds before the temperature reaches  $400^{\circ}\text{C}$ .

#### 4.2.1 Evaluation of the Accuracy and parameter Sensitivity of the Transient Model

The dimensionless temperature will be limited by a constant around 1, remember the scaling  $T = \frac{\theta - \theta_{1,in}}{\theta_{1,in}}$ , hence equation 54 can be used. The value of  $G$  for the above results is  $G = 6$ , which results in an error bound by  $|e(t)| \leq \frac{1e^{-6}}{1-e^{-6}} = 0.0025$ . In order for the truncation error to be of the same order the upper limit of the sum, in equation 52, is set to 700. Higher accuracy can of course be achieved, increasing  $G$  is an easy task but to match this, the upper limit of the sum also has to be increased, which means that the calculations are getting very time demanding.

In order to show the importance of including enough terms in the sum, the methane in-signal is shown when calculated with the upper limit as either 70 or the upper limit as 700. The result is shown in Figure 27. Both plots tries to represent the same driving data, but as seen there is a large difference between them, where the upper limit of 700 gives a much better representation of the driving data. To test the model it is run with different parameters. In Figure 28a the model

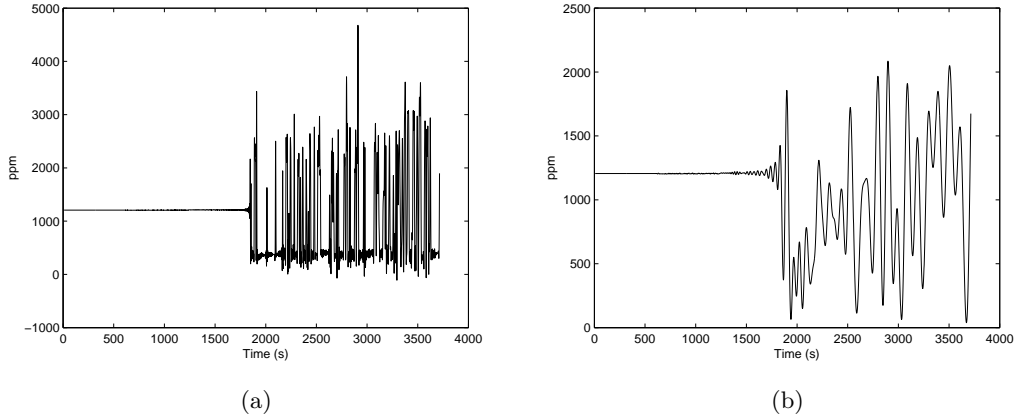


Figure 27: Comparing the methane-signal with different upper limits of the sum (a) 700 (b) 70.

is run with the constant in-data but with different  $h$  values. It can clearly be seen that the  $h$  value has a big impact on the final temperature, a higher  $h$  value will give a higher temperature into the catalyst. In Figure 28b the response of the temperature into the catalyst when the inlet temperature is changing is once again shown, but this time the density of the heat exchanger is divided by two. The response is still quite smooth, but comparing it with Figure 23b it shows that changing the in-temperature has a bigger impact on the temperature to the catalyst when the density is lower. In Figure 28c the model is run with constant values but with the data for the gas, density, heat capacity, viscosity and thermal conductivity, at  $300^{\circ}C$  instead of as earlier  $400^{\circ}C$ . This is done to test the assumption that the data for the gas is independent of the temperature. Comparing Figure 28c with Figure 21a it can be seen that running the model with with the data at different temperatures, clearly affects the result. The idea is that choosing an average temperature will minimize the error, but not having the temperature dependence of the gas properties in the model will introduce an error. In Figure 28d the model is run with changing methane concentration, but with the plates being of double the thickness. Comparing the result to Figure 22b it can be noted that it takes longer time to reach steady state, the system has barely reached steady state once the in-data is applied. But once warm it can be seen that instead of varying between  $400 - 600^{\circ}$  it changes between  $445 - 575^{\circ}$ , with smaller fluctuations in between.

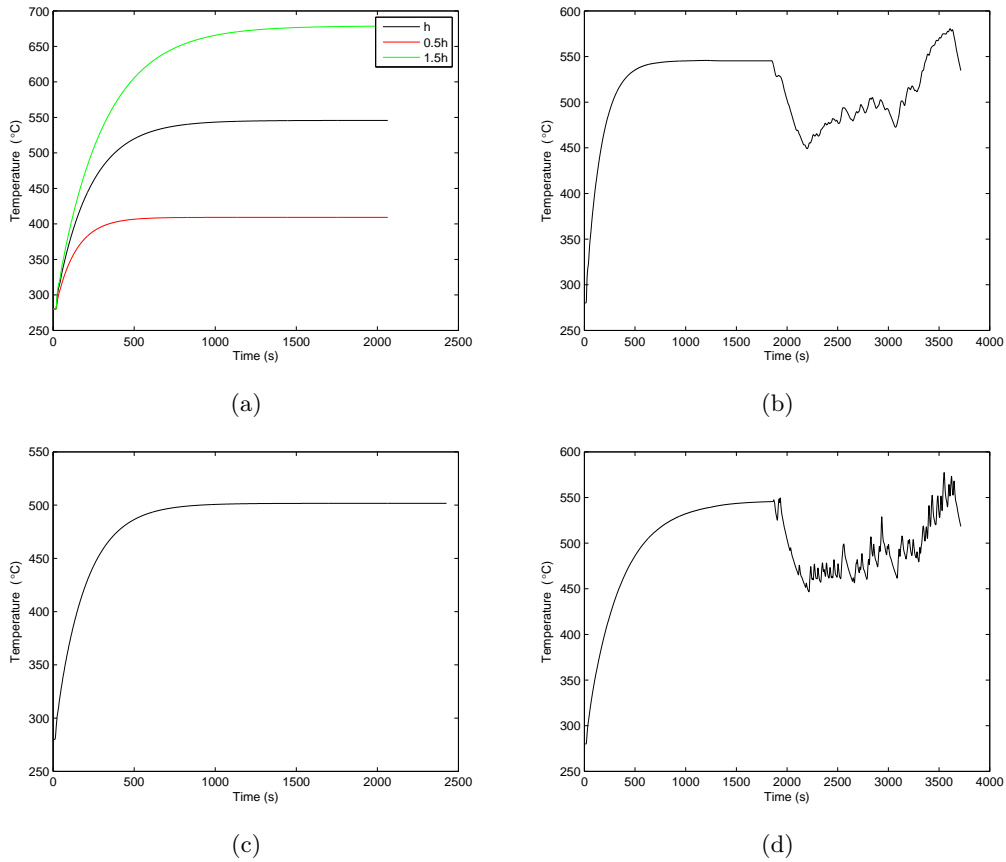


Figure 28: Testing the model (a) the dependence on  $h$  (b) lower density (c) parameters evaluated at a different temperature (d) double plate thickness.

#### 4.2.2 Calculation time

To use the transient model with constant in-data and with the lower limit set to 70 takes around two minutes. Increasing the accuracy by setting the upper limit to 700 increases the computation time to around 15 minutes. But what really makes the calculations time demanding is to implement the driving data. Each of the changes in the data is seen as a step change, such that when the data is Laplace transformed it becomes a sum of exponential functions divided by the Laplace variable  $s$ , i.e.  $\frac{ae^{-t_0s} + be^{t_1s} + \dots}{s}$ . The data consists of around 1800 values, meaning that the boundary condition for the methane and the in-temperature will consist of a sum of 1800 exponential functions that has to be calculated for each time step. This means that when both the methane concentration and the inlet temperature are changing it takes around six hours to solve for the transient model, where the computer had a single processor of 2.83 GHz.

### 4.3 CFD Simulations

Simulations were performed over several different gap distances. These simulations were done with air, simulated with a chevron angle of  $80^\circ$ .

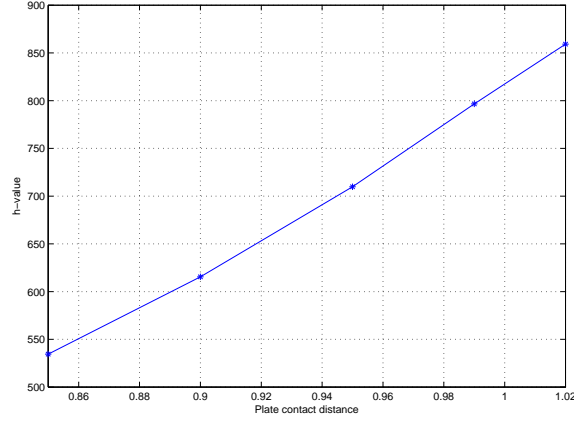


Figure 29: Heat coefficient values for different gap distances.

From Figure 29, it can be seen that the h-values increases linearly as the gap between the corrugations gets smaller. The h-values were calculated from the Eq. 9. The Q value was gathered by integrating the heat transfer flux over the outer walls of the geometry in Fluent. The area was taken from the outer walls of the geometry and the  $\Delta T$  was derived by subtracting the mass-averaged temperature over the interior of the geometry from the temperature of the outer walls.

In Figure 30 it can be seen that the velocity was increased in the narrow passages as the gap between the two plates decreases.

In order to compare the simulations results, the simulated h-value was compared to different correlations values for h found in the literature. This was tested for simulations for both air and water. All of the simulations were performed with no gap between the plates. Identical compound properties were used for the simulations and the correlations. Two different Chevron angles were compared,  $30^\circ$  and  $80^\circ$ . The mass averaged velocity from the different simulation cases were used as input data for the Reynold number in the correlations. Data from simulations and correlations can be found in Table 7.

Table 7: Comparison between simulation and correlations.

Simulation case	Chevron angle	Compound	Simulation h-value	Correlation 1 [14] h-value	Comparison to simulation value (%)	Correlation 2 [9] h-value	Comparison to simulation value(%)
Full width	$30^\circ$	water	6984	4545	65	6297	90
Full width	$30^\circ$	air	253	159	63	192	76
Symmetric segment	$30^\circ$	water	8979	4481	50	6227	69
Symmetric segment	$30^\circ$	air	287	154	54	186	65
Symmetric segment	$80^\circ$	water	23061	-	-	21109	92
Symmetric segment	$80^\circ$	air	856	-	-	716	84

From Table 7 it became clear that the simulations with a Chevron angle of  $80^\circ$  follows the

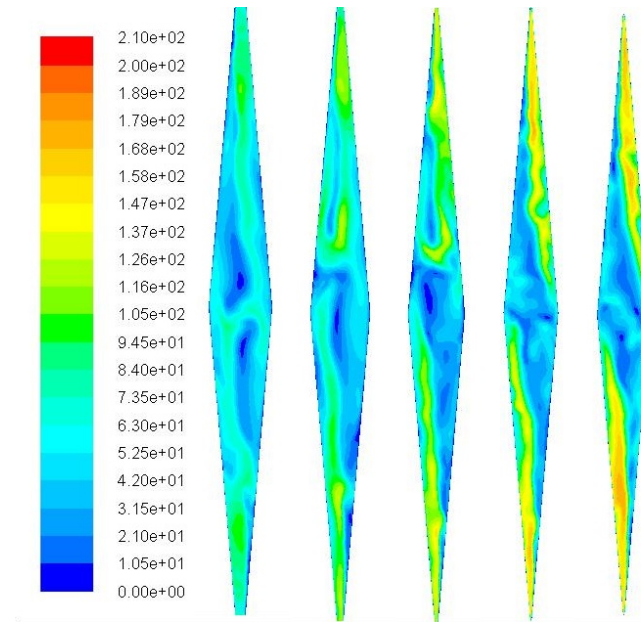


Figure 30: Velocity profiles over the inlet with gap distances of 0.85, 0.9, 0.95, 0.99 and 1.02.

Table 8:  $\phi$ -value adjustment

Simulation case	Chevron angle	Compound	Simulation h-value	Correlation 1 [14] h-value	Comparison to simulation value (%)
Full width	30°	water	6984	7771	111
Full width	30°	air	253	273	108

correlations values well, especially in the case simulated with water. The 30° Chevron angle simulations shows larger differences between the simulation values and the correlations for both compounds.

From Table 7 it becomes clear that the different width of the simulations affects the heat coefficient to some extent. The h-value for the simulation over the full width of the heat exchanger showed a lower value than for the simulation over the symmetric segment.

In Table 8, the  $\phi$ -value, defined by the real area divided by the projected area, for correlation 1 is altered from 1.11 to 1.29. The resulting h-values can be seen in comparison with the h-values from the simulated cases.

Path line profiles of the simulations are presented in the Figures 31, 32, 33 and 34, all colored by temperature (K).

By comparing Figures 31 and 32, one can see that the flow profiles for the different simulations vary. In Figure 31, the path lines are following a curved shape as the flow changes direction as it hits the sides of the geometry. In Figure 32 the full width of the heat exchanger is simulated and hence the flow profile follows a more criss-crossed formed pattern. As can be observed, the flow from one of the symmetry segments in this simulations often travels to neighboring segments by following the corrugation channels. Noticeable is also that the flow profile in the right part of the

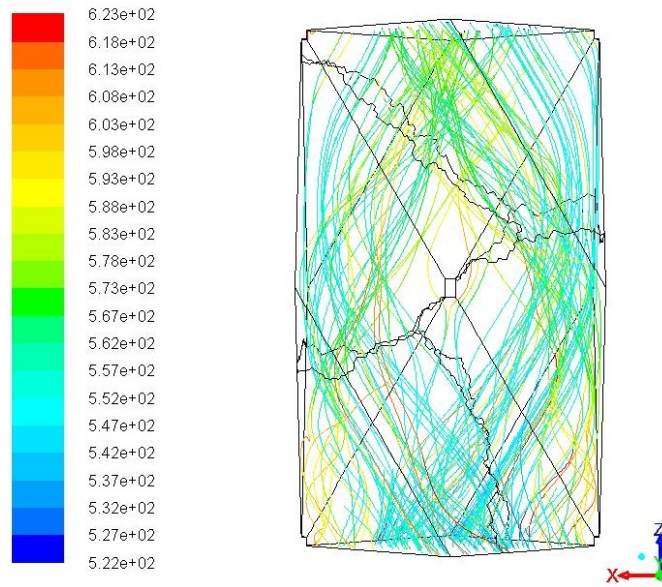


Figure 31: Path line figure for the symmetric segment of the heat exchanger.

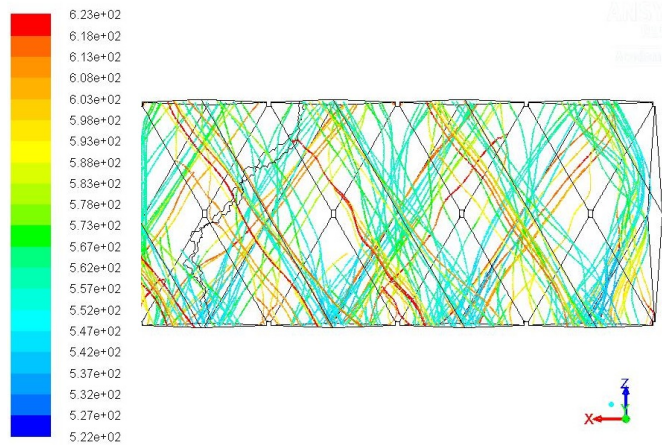


Figure 32: Path line figure for the whole width of the heat exchanger, showing the four rightmost segments.

rightmost segment in this simulation differs from the rest of the flow by showing a curved path, similar to the profile in Figure 31. The reason for this is the side wall of the heat exchanger, providing this part with similar boundary conditions as in Figure 31. In Figure 33, one can see the same flow tendencies in the middle of the heat exchanger as were observed in Figure 32, close to the side wall. It is also noted that a few of the path lines in Figure 32 are a bit warmer compared to the ones in figure 31. These path lines display the flow closest to the outer walls of the heat exchanger.

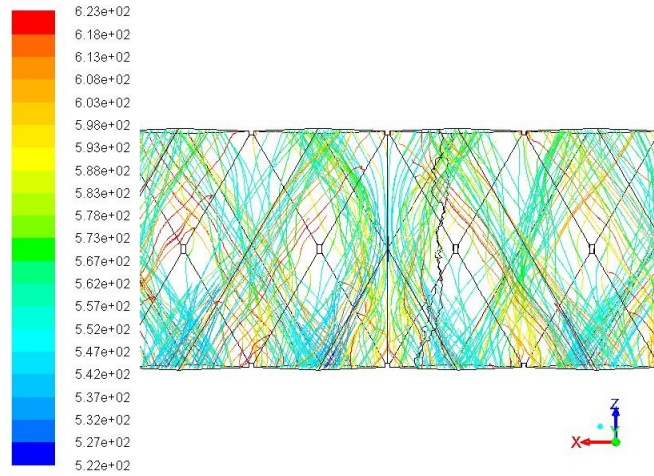


Figure 33: Path line figure for the whole width of the heat exchanger, showing the middle segments.

Figure 34 present the path lines in a symmetric heat exchanger segment with an Chevron angle of  $80^\circ$ .

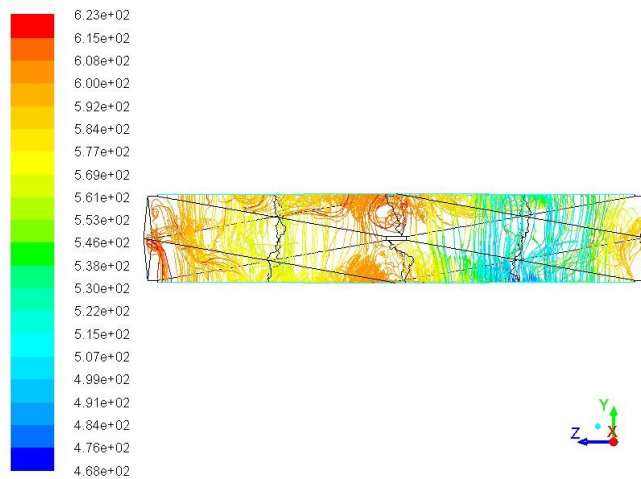


Figure 34: Path lines for the  $80^\circ$  symmetric segment of the heat exchanger.

By comparing Figures 31 and 34 which both are simulations over symmetric segments of the heat exchanger, it shows that the flow patterns are significantly different. The criss-cross shaped flow shown in Figure 31 have changed in Figure 34 towards a a flow that instead tends to roll over the corrugations. From Figure 34 one can see that swirls are formed before and after the areas were the plates connects in the geometry. This phenomenon was not observed in the geometry with a Chevron angle of  $30^\circ$ . As seen in Figure 34, the temperature in this area is also higher than elsewhere in the geometry.

The thermal boundary layer in the simulation with a Chevron angle of  $30^\circ$  were observed to have a thickness of about 0.12 mm at its thinnest point. For the simulations with a Chevron angle of  $80^\circ$ , the thermal boundary layer were as thin as approximately 0.02 mm. The heat transfer is observed to be at the highest close to the corrugated plate downstream in the flow direction for both of the Chevron angles.

## 5 Discussion

### 5.1 Transient Simulations

By simply looking at the steady state model it seems like an easy task to implement an heat exchanger such that good temperatures can be reached in the catalyst. When the average conditions are applied to the steady state model it is the limit on the pressure drop that sets the size of the heat exchanger, rather than the temperature out from the exchanger. In order to get a pressure drop that is below  $10kPa$  62 channels were needed, which resulted in temperature of almost  $530^\circ C$  which is more than enough to keep good conversion in the catalyst. But the conditions are often far from steady, they are in fact changing very rapidly. Hence to be able to predict the temperature into the catalyst the transient model is applied. It can be seen that when the transient model is run with the same constant values as the steady state model a temperature of around  $545^\circ C$  is reached, i.e. a bit higher than for the steady state model. The reason for this is that conduction through the plates is set to infinity in the transient model, i.e. the model will give a slight over prediction of the temperature.

However once the transient in-data is applied it is apparent that it is not as easy to design the heat exchanger. The results shows that the temperature out from the heat exchanger is more dependent on the concentration of methane than on the inlet temperature. The response from changing the inlet temperature is slower and hence only the larger average changes will be visible on the outlet temperature. The response from changing the concentration of methane is quicker, every time the amount of methane is decreasing the temperature into the catalyst is decreasing. It is hence important that the heat exchanger always gets some methane, in order to avoid that the temperature drops so low that the methane will stop reacting. By looking at the result when all in parameters are changing, Figure 24b, it seems like the design with 62 channels and a chevron angle of  $30^\circ$ , if preheated almost will be enough. The inlet temperature of around  $150^\circ C$  and the concentration of methane that is close to zero gives at the start a large temperature decrease. But after that the temperature stays high enough to keep good conversion of methane, despite the rapidly changing conditions at the inlet.

If longer periods of low inlet temperature and low amount of methane are expected to occur frequently, a better heat exchanger will be needed. This is achieved by either increasing the chevron angle, i.e. increasing the  $h$ -value, or by increasing the size of the heat exchanger. The result of these two changes is shown in Figure 25. Increasing the  $h$ -value means a redesign of the plates and does hence not require any more space, and can from the result be seen to give a large increase of the temperature. However at high load driving conditions this will result in temperatures around  $700^\circ C$ , which might be so high that the catalyst will be damaged. Increasing the  $h$ -value by 50% does also mean that the pressure drop is increased with a factor 5. Adding another 30 channels means that additional space for the heat exchanger has to be made in the truck, but the results shows that the heat exchanger will keep the temperature higher during the period of low inlet data, but not too high during the high load conditions. More channels also has the additional advantage that the pressure drop will decrease. Another option to keep the heat is to

increase the thickness of the plates in the heat exchanger, i.e. increasing the thermal mass. This has the disadvantage of requiring longer time for preheating the system and worse conduction through the plates, but Figure 28d indicates that the more of the heat will be kept in the system.

If the transient boundary conditions are applied without first preheating the gas, Figure 26, it takes a long time before the temperature gets above  $400^{\circ}\text{C}$ . This is even with all the methane reacting despite the low temperature. In a real case there would be other substances that would react, but the conversion of methane would be very low at the starting temperatures. However methane is the major contribution to the increase of temperature and the result for the upstart process will hence be an overestimation of what will happen. It therefore seems like it is needed to preheat the gas such that the reaction of methane will start, and preferably the gas should be preheated well above the temperature needed for the methane to react, such that the system has some margin. Looking at the results from the transient simulation it seems like it would be good to have an electric heater that has the capacity to increase the temperature of the gas with around  $200^{\circ}\text{C}$ . Given a mass flow of  $0.2\text{kg/s}$  the capacity of the electric heater can be calculated to  $40\text{kW}$ .

## 5.2 CFD

From Figure 29 it becomes clear that the gap distance greatly affect the heat transfer coefficients for the different simulations. The effect of the gap distance could be seen to be almost strictly linear. This implies that gap distances between the plates should be avoided when performing simulations even if it simplifies other parts of the project, such as the meshing. Even for a very thin gap distance of 0.99, the difference in the heat transfer coefficient compared to the case where the plates were in contact were about 10%. The velocity increased when the gap became smaller which probably resulted in increased swirl formations.

From Figure 34 one can see that the temperature close to the inlet are locally as low as 468K, even if the inlet conditions were set to 553K. This was possible because the periodic inlet temperature was mass-weighted averaged over the inlet area, which therefore enables the local temperature deviations.

In Figure 32 and 34, the expected flow profiles can be observed, indicating that it is possible to simulate plate heat exchangers with the use of CFD software. In Figure 33, it is possible to see that in the center of the heat exchanger, i.e. where the corrugations merge together, that the flow profiles is changing. Only a very little part of the flow travels to the opposite side of the geometry. As the flow from both directions collides in the middle, the major part of the flow does then revert back towards the same side it came from. One can by comparing this flow profile to the flow profile close to the side wall of the heat exchanger see many similarities. This points in the direction that the whole width of the heat exchanger does not need to be simulated. Simulating half the width of the heat exchanger would therefore be sufficient in order to create results similar to those created by a full width simulation.

Regarding the correlations which the simulation values were compared to, the simulations which had an Chevron angle of  $80^{\circ}$  showed the best compliance with the chosen correlations. During the simulations with a Chevron angle of  $30^{\circ}$ , the simulated values for the convective heat transfer coefficient were higher for both air and water. It is also observed that the simulations are showing better agreement with both of the correlations in the case when water was simulated. It is also possible to conclude that the geometry with the smaller width produced a higher h-value. This is

an expected outcome, and the reason for this is that the simulations in the smaller width segment case collides with the side walls of the geometry more frequently, causing a change in direction and an increased replenishment of the boundary layer. In the simulations with a Chevron angle of  $80^\circ$ , it was shown that the h value in the simulations with water was closer to the correlation value, compared to air. However, by observing Table 7 it becomes clear that the convective heat transfer coefficient differs between the simulations and the correlations. Differences can also be observed between the different correlations. One of the major reasons to the differences between the h-values in Table 7 is believed to be differences in the geometries. Correlation 1 is valid for sinus shaped corrugations, while the simulations were done with a V-shaped pattern. The amplitude and the period of the correlations will determine the  $\phi$ -value for the chosen geometry. However, different geometrical setups of the corrugations, i.e. sinus shapes and V-shapes, will have a different value for  $\phi$ , given the exact same amplitude and period. An example of this is the simulation performed in this thesis, which were done with a  $\phi$ -value of 1.11, while Muley and Manglik presents almost identical amplitude and period of their corrugations, but with a  $\phi$ -value of 1.29 [14]. Sine-shaped correlation will have difficulties to estimate simulations done with V-shaped corrugations. However, an attempt to compare the simulations with the correlations presented by Muley and Manglik was performed. By changing the correlations  $\phi$ -value from 1.11 to what seems to be the equivalent  $\phi$ -value for sine-shaped corrugations, 1.29, the new correlation values showed significant improvement and the difference between the values ended up was calculated to be less than 10%.

It should be noted that the correlation chosen as a comparison in the case with a Chevron angle of  $80^\circ$  actually were valid for simulations with a Chevron angle of  $75^\circ$ . Since the h-value tend to increase as the Chevron angle increases from  $75^\circ$  to  $80^\circ$ , it is believed that the simulated h-values would have shown an even better match, had the correlation been for  $80^\circ$  instead since both of the simulated h values were slightly higher compared to the correlation.

The thermal boundary layer were discovered to be smaller for the simulations with a higher Chevron angle. This was expected since a higher Chevron angle forces the flow to tumble over the corrugations rather than following the corrugation channels. This causes swirls that replaces the fluid close to the outer walls of the heat exchanger with fluid which previously were located in the bulk flow, thereby decreasing the thickness of the thermal boundary layer. A more rapid replacement of the boundary layer leads to shorter duration time close to the walls for the fluid, which in turn leads to continuously high temperature difference between the fluid and the walls. This enhances the heat transfer for the heat exchanger, which in turn could be seen in shape of the higher value for the convective heat transfer coefficient.

## 6 Conclusions

The literature study concludes that it is most efficient to use a sequential system instead of having the catalyst integrated in the heat exchanger. Preferably a system of bypasses should be used such that the flow during cold start directly will enter the catalyst. But even with the bypass system the literature study suggests that an electric heater is needed in order to get the system started.

The results from the transient model shows that the system will take very long time to reach the temperature of ignition for methane, which is in agreement with the literature study and confirms that additional heating is needed during cold start.

The steady state model suggests that for the pressure drop to stay below  $10kPa$  a plate heat exchanger with a projected area of  $0.65 \times 0.17 m$  and a chevron angle of  $30^\circ$  will require 62 channels. Applying the transient model with this heat exchanger and typical driving conditions gives that, if preheated, the temperature will most of the time stay above  $400^\circ C$ . If it is required that the heat exchanger should be able to handle longer periods of low inlet temperature and low concentration of methane, the most effective way is to change the chevron angle such that the  $h$ -value is increased. This will however lead to an increased pressure drop and might also give too high temperatures in the catalyst during high load conditions. The other options is to increase the size of the heat exchanger which also has the advantage that it will lead to a lower pressure drop.

The simulated flow profiles showed clear similarities with previously reported experimental flow patterns, confirming CFD as a valid tool for flow analysis of plate heat exchangers. The convective heat transfer coefficient values are in reasonable agreement with the correlation values. From this, a conclusion can be drawn that it is of great importance for the geometrical construction to be similar to the geometrical construction from which the correlation was based upon.

Simulations with gap between the plates were tested and showed poor compliance with the simulation case where the plates were in contact, and should therefore be avoided. It has also been shown that the full width of heat exchanger geometry is needed for the simulations with lower Chevron angles.

## 7 Future Work

The thesis presents a mathematical solution that solves the stated partial differential equations analytically, up to the point of the numeric inversion of the Laplace transform. But in order to use the mathematical procedure some assumptions had to be made. It is however possible to include some of them and still use the same mathematical framework. It is for example possible to include terms modeling conduction through the plates, the axial dispersion within the channels, heat leaking to the surrounding or the flow maldistribution from channel to channel. But all of these terms adds more complexity to the partial differential equations and was for the given time frame neglected, but they should be added for more precise predictions of the performance of the heat exchanger.

The model could further be extended by adding more species, such as carbon monoxide, that could react and generate heat in the catalyst. But for this to really be interesting it would be needed that the different species starts to react at different temperatures. With the reaction of methane and other substances being temperature dependent the upstart process could be simulated in a more correct way, instead of the current over prediction. But including this means that the mass balance over the catalyst will be temperature dependent, and hence no longer have an analytical solution. Typically the temperature dependence comes from the reaction constant  $k \propto e^{-\frac{E_a}{RT}}$ . The nonlinear dependence on the temperature will be a challenge for the current mathematical framework to solve, but a solution method that includes the temperature dependence is something that should be included in a future model. One way to solve this problem could be to approximate the nonlinear term with a linear expression for the kinetics of the reaction of methane. Another way to improve the model would be to add an electric heater to

the system. Preheating the system is currently done by running the system with constant values before the transient data is applied. This does however take some time, and it would not be too hard to add a source term to the differential equations that would represent an electric heater, where it would be possible to choose the power of the electric heater and determine for how long time the electric heater should be turned on.

One of the limitations in the CFD simulations was that the wall temperature was set as a constant. In order to improve and verify the simulations, it would be of interest to conduct simulations consisting of a warm and a cold stream in the heat exchanger separated with a corrugated plate. If performed, it would be of interest to perform transient simulations with alternating mass flow and temperatures to observe how these affect the thermal boundary layer of the heat exchanger.

## References

- [1] Heavy-Duty Truck and Bus Engines –Regulatory Framework. *DieselNet*. (<https://www.dieselnet.com/standards/eu/hd.php>). Accessed 2014-06-17.
- [2] New Trucks – Volvo FM MethaneDiesel. *Volvo Trucks Global*. (<http://www.volvotrucks.com/trucks/global/en-gb/trucks/new-trucks/Pages/volvo-fm-methanediesel.aspx>). Accessed 2014-06-17.
- [3] Overview of Greenhouse Gases. *EPA – Untied States Environmental Protection Agency*. (<http://epa.gov/climatechange/ghgemissions/gases/ch4.html>). Accessed 2014-06-17. Boston.
- [4] Rink, M., Eigenberger, G., Nieken, U.(2012) Heat-Integrated Exhaust Purification for Natural Gas Engines *Chemie Ingenieur Technik*. Volume 3 pp. 421–426.
- [5] Heed, B., Wingård,S.(2009) Catalytic converter with good conversion for methane *Dessau Gas Engine Conference*; March 26-27,2009, Gothenburg.
- [6] Bernnat, J., Rink, M., Tutt, U., Danner, T., Nieken, U., Eigenberger, G. (2009) Heat-Integrated Concepts for Automotive Exhaust Purification. *Topics in Catalysis*.,Volume 52, Issue 13-20, pp. 2052–2057.
- [7] Rink, M., Eigenberger, G., Nieken, U.(2013) Comparison of Two Different Heat-Integrated Exhaust Purification Devices for Monovalent CNG Engines *Springer Science+Business Media New York*. Volume 56 pp. 421–426
- [8] Hewitt, G.F.(2011) Plate Heat Exchanger Theory *Design of Industrial Energy Equipment* ed. Chalmers University of Technology- Department of Energy and Environment Gothenburg, Sweden.
- [9] Wang, L., Sundén, B., Manglik, R.M. (2007) *Plate Heat Exchangers: Design, Applications and Performance*. Ashurst Lodge, Ashurst, Southampton, UK: WIT Press.
- [10] Gullapalli, V.S. (2013) *Estimation of Thermal and Hydraulic Characteristics of Compact Brazed Plate Heat Exchangers*. Lund: Lund University.
- [11] Focke, W.W., Knibbe, P. G. (1986) Flow Visualization in parallel-plate ducts with corrugated walls. *Journal of Fluid Mechanics*, Volume 165, pp. 73-77.
- [12] Focke, W. W., Zacharioiades, J., Olivier, I. (1985) The effect of the corrugation inclination angle on the thermohydraulic performance of plate heat exchangers. *International Journal of Heat mass transfer*, Volume 28, Issue 8,pp. 1469-1479.
- [13] Zimmerer, C., Gschwind, P., Gaiser, G., Kottke, V. (2002)Comparison of heat and mass transfer in different heat exchanger geometries with corrugated walls. *Experimental Thermal and Fluid Science*, Volume 26, Issue 2-4, pp. 269-273.
- [14] Muley, A., Manglik, R. M. (1999) Experimental Study of Turbulent Flow Heat Transfer and Pressure Drop in a Plate Heat Exchanger With Chevron Plates. *Journal of Heat Transfer*, Volume 121, Issue 1, pp. 111-117.
- [15] Welty, J.R. Wicks, C.E. Wilson, R.E. Rorrer, G.L.(2007) Fundamentals of Momentum, Heat, and Mass Transfer. Fifth Edition Corvallis, Oregon: Wiley.

- [16] Sarit, K. Murugesan, K. (2000) Transient response of multipass plate heat exchangers with axial thermal dispersion in fluid *International Journal of Heat and Mass Transfer* Volume 43 pp. 4327-4345.
- [17] Dwivedi, A. K. Das, S.K.(2007) Dynamics of plate heat exchangers subject to flow variations *International Journal of Heat and Mass Transfer* Volume 50 pp. 2733-2743.
- [18] Srihari, N. Prabhakara Rao, B. sunden, B. Das, S. K.(2005) Transient response of plate heat exchangers considering effect of flow maldistribution *International Journal of Heat and Mass Transfer* Volume 48 pp. 3232-3243.
- [19] Andersson, B., Andersson, R., Håkansson, L., Mortensen, M., Sudiyo, R., van Wachem, B. (2011) *Computational Fluid Dynamics for Engineers*. Cambridge University Press, Cambridge.
- [20] Heck, R. H. Wei, J. katzer, J.R.(1976) Mathematical modeling of Monolithic Catalysts *AIChE Journal* Volume 22, Issue. 3 pp.477-484.
- [21] Hayes, R:E. Kolaczkowski, S.T. (1999) A study of Nusselt and Sherwood numbers in a monolith reactor *Catalysis Today* Volume 47, Issues 1-4, pp. 295-303.
- [22] Abate, J. Choudhur, G.L. Whitt, W.(1999) An introduction to numerical inversion and its application to probability models. *Computational probability* ed. Grassman, W. pp 257-323 Boston: Kluwer.
- [23] Kanaris, A.G., Mouza, A. A., Paras, S. V. (2009)Optimal design of a plate heat exchanger with undulated surfaces. *International Journal of Thermal Sciences.*,Volume 48, pp. 1184–1195.